Interplanar Coupling and Superconductivity in $(Cu_{½}TI_{½})Ba_2(Ca_{2-x}K_x)Cu_3O_{10-\delta}$ (x=0, 0.5, 1, 1.5) Samples

JAVERIA OWAIS RAZA

DEPARTMENT OF PHYSICS

QUAID-I-AZAM UNIVERSITY

ISLAMABAD, PAKISTAN

2023

In the name of ALLAH the Most Gracious, the most Merciful

Interplanar Coupling and Superconductivity in $(Cu_{\frac{1}{2}}TI_{\frac{1}{2}})Ba_2(Ca_{2-x}K_x)Cu_3O_{10-\delta}$ (x=0, 0.5, 1, 1.5) Samples

A dissertation to the physics department at Quaid-i-Azam University in Islamabad as a partial fulfillment of the requirement for the degree of

Master of Philosophy

In Physics

Materials Science Laboratory

Department of Physics

Quaid-e-Azam University

Islamabad, Pakistan

2023

This is to certify that **Ms. Javeria Owais Raza** D/O **Abdul Aziz** has carried out the experimental work in this dissertation under my supervision in **Materials Science Laboratory**, Department of Physics, Quaid-i-Azam University, Islamabad and satisfying the dissertation requirement for the degree of Master of Philosophy in Physics.

Supervisor

Dr. Syed Hamza Safeer Gardezi
Department of Physics,
Quaid-i-Azam University,
Islamabad, Pakistan.

Submitted through

Chairman

Prof. Dr. Kashif Sabeeh
Department of Physics
Quaid-I-Azam University Islamabad, Pakistan.

DEDICATED

TO

My Encouraging Parents and Extremely Supportive Husband

ACKNOWLEDGEMENTS

All the praises to **Almighty ALLAH**, the most merciful and the sovereign power, who enabled me to successfully accomplish this research work. I humbly send DAROOD-O-SALAM to **Holy ProphetMuhammad (P.B.U.H)** who shall remain forever a source of guidance and knowledge for humanity.

My deepest gratitude to my supervisor **Dr Syed Hamza Safeer Gardezi,** for his unwavering support during the research tenure. This endeavor would not have been feasible without his guidance, cooperation, and encouragement. I feel really overwhelmed on the completion of my research work under his supervision. My sincere gratitude goes toward my professor **Dr. Nawazish AliKhan** for his immense knowledge and guidance.

I am very grateful to my parents (**Abdul Aziz** and **Ishrat Nazir**) who provided me with every opportunity to learn, grow and always appreciated me. I thank them for encouraging me, guiding me and being there to strengthen me with confidence every time I felt weak or discouraged.

My special thanks to my Husband (**M. Rizwan**) for being immensely supportive and affectionate for my studies and career. Life’s challenges are easier to face when you are by my side. I extend my sincere gratitude toward my siblings (Sidra Owais and Mashood Ahmed) for their prayer support and encouragement.

Special thanks to my senior Iqra for guiding me a lot and also helped in editing as well formatting the thesis. My humble and heartfelt gratitude is reserved for my lab fellows Aqsa, Maria and Mehwish for their assistance. I will never forget the time I spent here.

Javeria Owais

Abstract

High-temperature superconductors (HTSC) is one of the most studied materials over the past century. The most noticeable family of the HTSC is the Tl-Ba-Ca-Cu-O cuprate family. There were many compounds prepared under this family of superconductors and still we are working on this compound. To further elaborate on the importance of this superconductor family we have doped alkali metal (Potassium) in this compound at Calcium sites by synthesizing $(Cu_{1/2}Tl_{1/2})Ba_2(Ca_{2-x}K_x)Cu_3O_{10-\delta}$(x=0, 0.5, 1, 1.5) superconducting samples. The samples were then characterized by X-ray diffraction, four-probe resistivity, scanning electron microscopy (SEM), and FTIR absorption measurements. These samples have shown high crystalline structure and followed the orthorhombic crystal and Pmmm space group. We found out that Potassium doping causes an initial increase in the c-axis length and unit cell volume, which is followed by a subsequent decrease as K doping is increased to 50%.This behavior is due to less electronegativity of K compared to Ca atoms. A subsequent decrease in the T_c(R=0K) and the T_c (onset) with the doping of potassium was observed which is due to the weaker interplanar coupling caused by doping of larger ionic size K atom compared to Ca. The apical oxygen mode of type Cu(1)-O_A-Cu(2) is softened with the doping of K in the final compound, as observed in the FTIR absorption measurements. Likely due to the increase in the c-axis that takes place in the charge reservoir layer blocks which elongates the bond length of Cu(1)-O_A-Cu(2) and hence the softening of this apical oxygen mode. The coherence length along the c-axis $\xi_{c(0)}$, and the London penetration depth $\lambda_{p.d}$ increase after doping of potassium and keep increasing as we increase the doping concentration of potassium. From here we can say the doping of the K at the Ca site the thickness of the interplanar layers increases thereby making the efficient transfer of the charge carriers to the conducting planes and hence increasing the density of the charge carrier in the conducting CuO_2 planes. The values of parameters such as B_{c0}(T), B_{c1}(T), J_c(0) are decreased with the increased K doping. This is because a smaller sized K causes the healing effect which reduces the microscopic pinning centers. We came to the conclusion that any alteration in the unit cell structure atom's mass or electronegativity with doping will significantly disrupt the interplanar coupling.

Table of Contents

Chapter 1: Introduction to Superconductivity

Chapter 2: Literature Review

Chapter 3:Experimental Techniques

Chapter 4: **Results and Discussions**

List of figures

Table of contents

Chapter#1

INTRODUCTION TO SUPERCONDUCTIVITY

The phenomena of superconductivity is discussed in this chapter. It covers the brief history of superconductivity, various types and properties of superconductors, as well as related terminologies and theories. The chapter concludes with several superconducting applications.

1.1 Superconductivity

'Superconductivity is a phenomenon where some materials emit magnetic field lines at low temperatures and many materials fully lose their electric resistance.'

The world of superconductivity has been opened by Kamerlingh Onnes' groundbreaking research on the electrical conductivity of mercury in 1911. Mercury (Hg) was the first material to exhibit superconductivity; its resistivity swiftly dissipated at 4K, which is at the critical temperature, the resistance immediately decreased to zero. Georg Bednorz and K. Alex Muller, made the first high-T_c superconductor discovery in 1986. For this significant advancement in the understanding of superconductivity in ceramic materials, they were given the 1987 Nobel Prize in Physics [1].

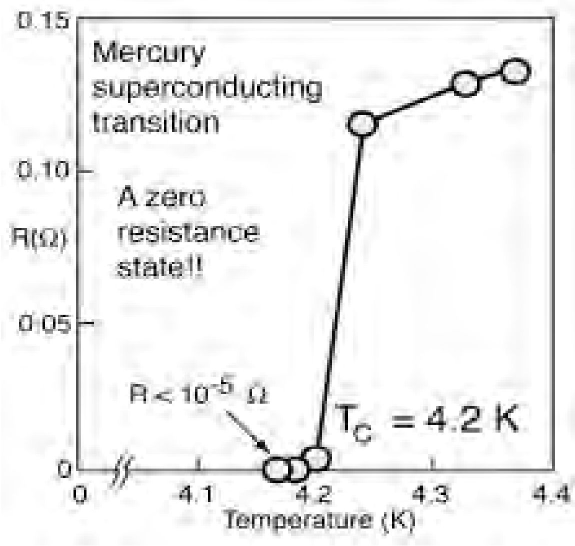

Fig 1.1: Temperature versus resistivity graph of mercury

In addition to opening up a new area for physics, this signaled a turning point in the evolution of electrical resistance. Superconductivity is simply defined as the loss of all resistance at a given temperature when the temperature of a material is reduced. This phenomenon only occurs at a critical temperature[2].

1.2Important characteristics of superconductors

The superconducting phase has two features, and superconductivity is the physical manifestation of quantum mechanics[3].

- Zero electrical resistance
- Perfect diamagnetism/Meissner's Effect

1.2.1 Zero Resistivity

The obstruction to electrons flow is known as resistance. Electrons regularly collide with atoms in the normal state, which results in the energy being transferred to the atoms of the lattice. The atoms begin to vibrate and release their energy as heat as a result. However, energy keeps escaping. Resistivity is defined as:

$$\sigma = ne^2 \frac{\tau}{m} \text{..................} (1.1)$$

$$\rho = \frac{1}{\sigma}$$

$$\rho = \frac{m}{n\tau e^2} \text{...............} (1.2)$$

Where, m ≡mass of electron, τ ≡ mean free time, e ≡charge on an electron and n≡ number density of electrons.

The lattice vibrations begin to freeze as the sample is gradually cooled. As a consequence, the vibrations within the electron-lattice are decreased. The electrical resistance in superconductors therefore totally disappears for infinite mean free time at a specific low temperature. Cooper pair is the name given to the pair of electrons that are bonded together by phonons in the superconducting state. This cooper pair can move without losing energy [4].

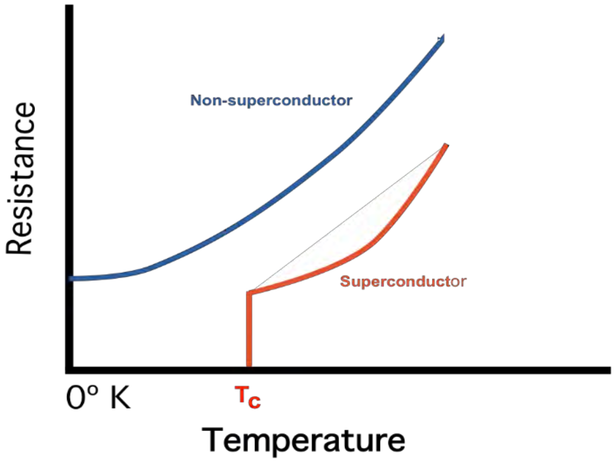

Fig 1.2: Resistance vs Temperature curve for superconductor.

1.2.2 Meissner effect

Meissner and Ochsenfeld (1933) found that once a sample has been immersed in a magnetic field and chilled until it reaches the superconducting threshold. The initial magnetic flux that exists is evacuated from the specimen. The above phenomenon is known as the Meissner effect. A massive superconductor behaves as a perfect diamagnet in a small magnetic field, exhibiting no magnetic induction in its core.

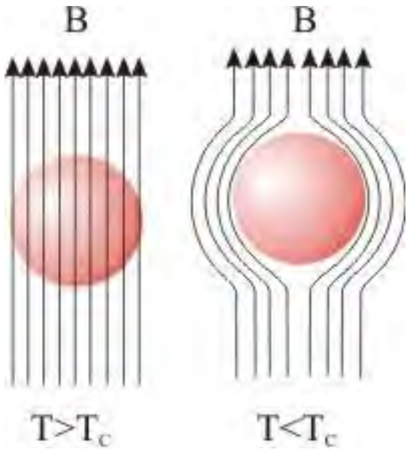

Fig 1.3: Meissner Effect

The magnetic field lines of induction are expelled out of the superconducting domain as the temperature falls below the transition point, causing the Meissner effect to occur (see figure1.3)

Since $$B = \mu_o (H + M) \ldots\ldots\ldots\ldots\ldots\ldots (1.3)$$

Magnetic field disappears in superconductors i.e., B=0

$$0 = \mu_o(H + M)$$

$$M = -H$$

Hence, the susceptibility is:

$$\frac{M}{H} = \chi = -1$$

$$\chi = -1 \ldots\ldots\ldots\ldots\ldots\ldots \text{(1.4)}$$

Since it represents the susceptibility of perfect diamagnetic material, this result demonstrates that superconductors have perfect diamagnetic behaviour[5].

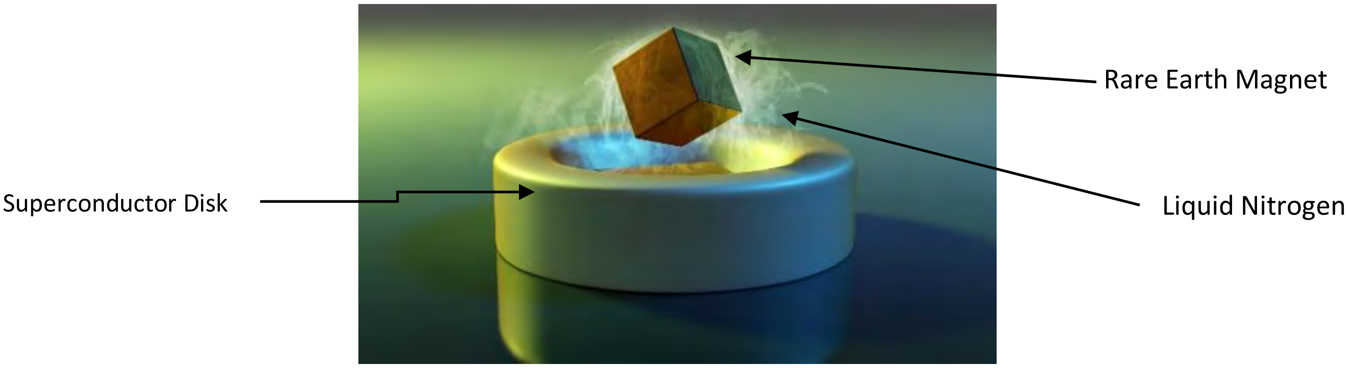

Fig 1.4: Superconductor as an ideal diamagnet repelling another magnet

1.3Conditions for Superconducting state

Three significant factors, notably the critical temperature (T_c), critical magnetic field (H_c), and the critical current density (J_c), are necessary for a sample to display superconductivity. These parameters must remain below their critical values for a sample to demonstrate superconductivity.

1.3.1 Critical Temperature (T_c)

The critical temperature or superconducting transition T_c is a point where a material loses resistance. [6]. According to BCS theory, below T_c, a Cooper-pair forms when two electrons in the same state are coupled by phonons. This Cooper pair has an integral spin and behaves similar to a boson. Above T_c, resistance increases, resulting in heat. This heat causes the Cooper-pairs to separate, destroying the material's superconductivity. The critical temperatures of some materials are mentioned in the table below.

Materials	**Critical temperature T_c (K)**
Hg	**4.6**
Nb	**9.3**
C_6Ca	**11.5**
V_3Si	**17.1**
Nb_3Sn	**18.3**
$TlSrLaCuO_5$	**40**
$YBa_2Cu_3O_7$	**90**
$TlBa_2Ca_2Cu_3O_9$	**120**

Table 1.1:*Critical temperatures of various superconductors*

1.3.2 Critical Current Density (J_c)

To avoid resistance during the transfer of a substantial current, superconducting cables can be used. Yet, the amount of current that can pass across these wires is constrained in certain ways. The amount of current flowing through a unit area of superconducting wires is called current density 'J'. When J > Jc, these wires no longer remain superconductors and become normal conductors. Kunzler first observed Jc in 1961 [7].

Temperature also affects critical current density. For practical purposes, J_c must be greater than $1000 A/mm^2$. At very low temperatures, thallium-based cuprate superconductors can achieve 106 to 107 A/cm^2.

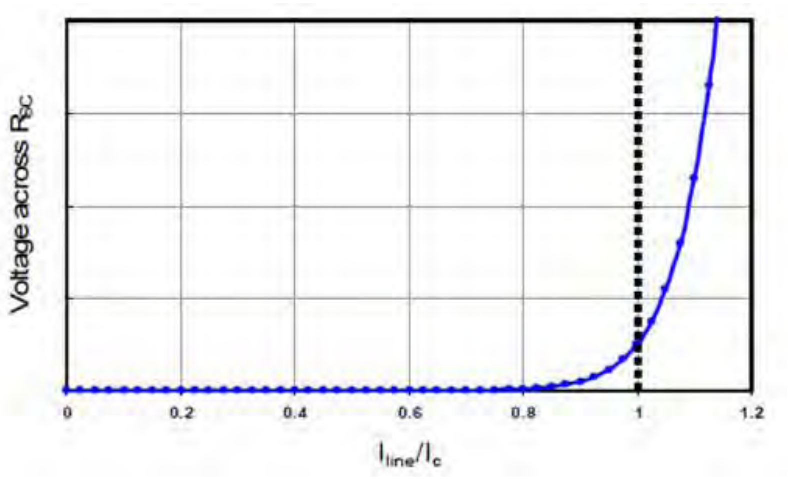

Fig 1.5: Voltage vs. Current graph for a superconducting wire

1.3.3 Critical Magnetic Field (H_c)

Superconductivity is affected by magnetic fields that are sufficiently potent. $H_c(T)$ is a measure for the temperature-dependent limit or crucial value of the imposed magnetic field required for eliminating superconductivity. A critical field reaches zero at a critical temperature: $H_c(T_c) = 0$. Figure 1.6 depicts how the threshold field for numerous superconducting components varies with temperature [5].

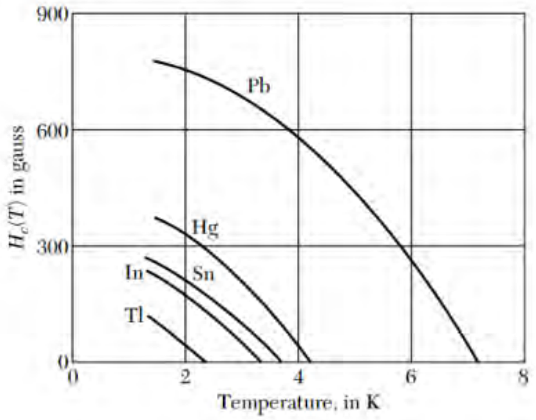

Fig 1.6: Experimental critical field Hc(T) vs temperature curves for numerous superconductors. A specimen is superconducting beneath the curve and normal above it.

1.3.4 Correlation among T_c, H_c and J_c

All three critical values are interconnected. J_c and H_c have their highest values at zero Kelvin. When the temperature reaches the critical point, however, both J_c and H_c become zero. A critical surface is obtained by plotting these three critical values. The material behaves as a superconductor inside the critical surface, but not outside of it[8].

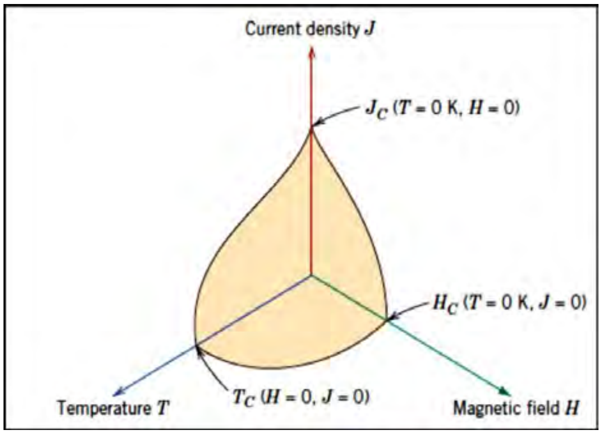

Fig 1.7: Critical surface phase diagram

1.4. Type I and II Superconductor

For the inaugural time, two researchers, L. Landau and V.L. Ginzburg suggested that two types of superconductors exist [10]. Based on magnetic characteristics, superconductors have been categorized in two types: type I and type II. Apart for niobium, all superconducting elements are included in Type-I superconductors. The other group, type-II superconductors, is made up of vanadium, metal alloys, and chemical compounds. This category also includes so-called high-Tc superconductors. The primary distinction among each of the categories is their varied responses to a magnetic field that surrounds them.

1.4.1. Type 1 Superconductors

Take a look at a superconductor's magnetization curve. Let's assume that the item being examined appears as a long cylindrical object under a transverse extrinsic magnetic field called H_o. The induction within the object remains constant as the field H_o develops; it maintains B = 0. When H_o approaches H_{cm}, superconductivity vanishes as the field enters the superconductor, and B = H_o. They are linked by the well-known expression:

$$B = H_o + 4\pi M$$

Here M defines the magnetic moment per cubic centimeter.

The profile of magnetization projected by a type 1 superconductor following the conditions established by the Meissner-Ochsenfeld experiment is shown in the figure 1.8 (a) (b) [5].

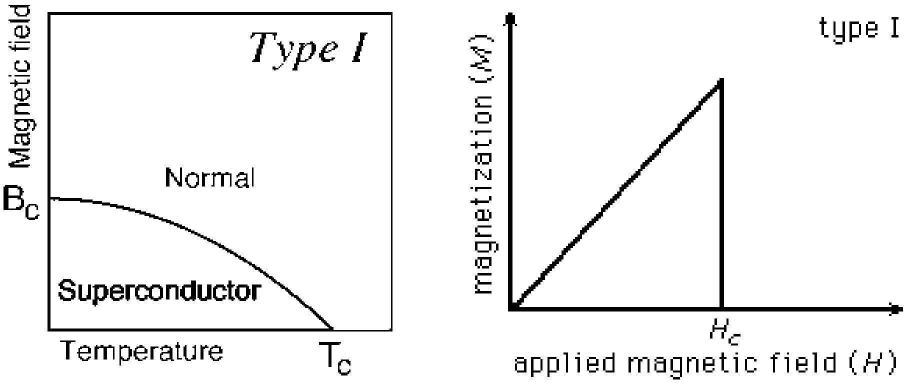

Fig 1.8 (a):H-T phase diagram of superconductors of type-I.**Fig1.8 (b)**: Magnetization vs. Applied magnetic field showing perfect diamagnetism

1.4.2. Type 2 Superconductors

For type II superconductors, the Meissner-Ochsenfeld phenomena does not exist as it does in type I superconductors. These materials are distinctive in the way that a field of magnets enters them. In the trajectory of a magnetic field, place a type II superconductor in the shape of an extensive cylinder. Beyond zero, the field is expanded.

Because the cylinder initially throws the entire field away therefore magnetic induction in the cylinder's center is zero. It suggests that the Meissner-Ochsenfeld effect appears first. However, starting with an exact field value, we will notice there is limited induction in the cylinder. It is known as the lower critical field and is represented as H_{c1}. While the exterior field H_o expands further, the induction increases till the standard field within the cylinder equals the outer field H_o as well as the cylinder returns towards its original form. That happens to take place at the higher critical field H_{c2}.

Nevertheless, superconductivity will persist in a thin surface layer even at $H_o > H_{c2}$ until Ho = 1.69 H_{c2}.This field is powerful enough to interfere with the superconductivity of the upper layer. The symbol for the third crucial field is H_{c3}.

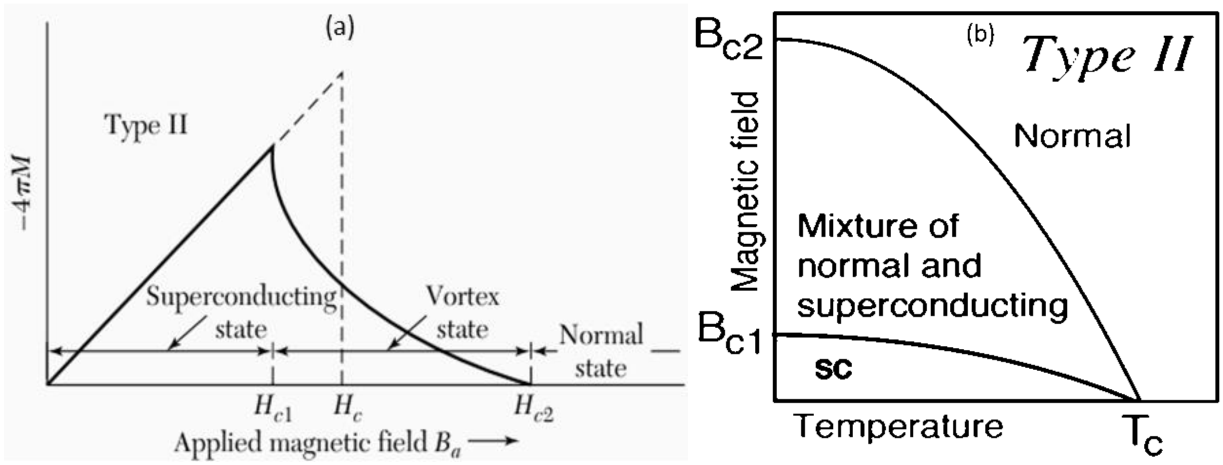

Fig 1.9(a) Type 2 superconductor's superconducting magnetization**Fig1.9(b)** H-T phase illustration

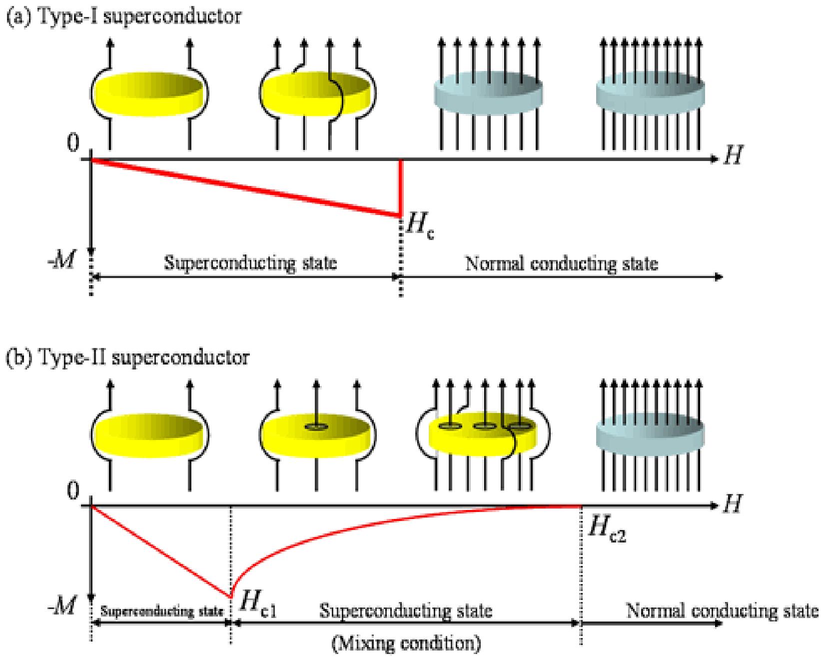

Fig 1.10: Comparison of Type 1 and type 2 superconductor in a magnetic field

1.5. Evolution of theory of superconductivity

To explain the physical phenomenon of superconductivity different theories were presented:

1.5.1. London Theory

Maxwells equations were unsuccessful in defining the Meissner effect in superconductors. Then, in 1935,the explanation concerning the macroscopic conduct of superconductors in the surrounding environment was provided by F. and H. London. They proposed a two-fluid model to explain how a superconductor might behave in a surrounding electromagnetic field. Suppose that there are two groups of free electrons in the superconductor:

- Conventional electrons with density n_n
- Superconducting electrons of density n_s

Here, n_n represents the concentration of ordinary electrons, whereas n_s represents the concentration of superconducting electrons. The entire electron density becomes: $n = n_n + n_s$

As, $T<T_c$,$n_n \rightarrow 0$ and $n_s \rightarrow$ maximum value

$T>T_c$, $ns \rightarrow 0$ and $n_n \rightarrow$ maximum value

Suppose that the superconducting electrons are not impacted by the electromagnetic fields because they both seem very minimal. Furthermore, consider that the no. of superconducting electrons n_s remains constant throughout.

In the presence of an electric field, the mathematical calculation for motion of superconducting electrons is:

$$n_s m \frac{dv_s}{dt} = n_s E e \quad \ldots\ldots\ldots\ldots\ldots\ldots\ldots (1.5)$$

Where e, m, v_s, and n_s denote electron charge, mass of electron, velocity of superfluid and number density.

$$dJ_s/dt = (n_s e^2/m)\, E \quad \ldots\ldots\ldots\ldots\ldots\ldots (1.6)$$

$$Where, \qquad j_s = n_s e v_s$$

The forementioned equation is recognized as London First equation. This equation implies that in a stationary condition, the superconductor has no electric field, i.e. when $dj_s/dt = 0$.

For evaluating the magnetic behaviour of the superconducting state, we shall use the Maxwell equation.

$$\nabla \times E = -dB/dt \ldots\ldots\ldots\ldots\ldots\ldots\ldots\ldots (1.7)$$

At E=0, B is constant, suggesting that the superconducting material has a homogeneous magnetic field. This finding, however, contradicts Meissner's effect idea. London proposed some modifications in the equation to eliminate the contradiction, the modified equation is

$$\nabla \times J_s = -\frac{n_s e^2 B}{m} \text{ ……………………… (1.8)}$$

The above formula is frequently referred to as the London second equation.

1.5.1.1 London penetration depth

As magnetic field is directed to superconductor's surface magnetic field lines can only sink to a certain depth, described as the London penetration depth and is indicated by a symbol $\lambda_{L.}$

From Maxwell's equation:

$$\nabla \times \mathrm{B} = \mu_o \mathrm{Js} \text{ ………………….. (1.9)}$$

Taking curl on both sides we get:

$$\nabla \times (\nabla \times \mathrm{B}) = -\frac{\mu_o n_s e^2 B}{m} = \frac{-1}{\lambda^2} B \text{………………… (1.10)}$$

Taking, $\lambda_L = (m_e / \mu_o n_s e^2)^{1/2}$

$$\nabla \times (\nabla \times \mathrm{B}) = \nabla(\nabla . \mathrm{B}) - \nabla^2 \mathrm{B}$$

Maxwell equation says $(\nabla . B) = 0$

$$\nabla^2 B = \frac{1}{\lambda^2} B$$

$$B = B_o e^{-x/\lambda_L} \text{ ………………… (1.11)}$$

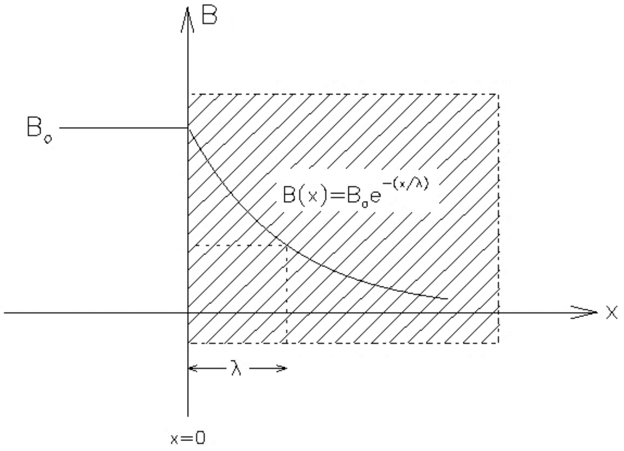

Fig 1.11: Magnetic field penetration within the superconductor

Penetration depth has been a function of temperature and mathematically written as,

$$\lambda(T) = \frac{\lambda(0)}{[1+(\frac{T}{T_c})^4]^{1/2}} \ldots\ldots\ldots\ldots\ldots\ldots\ldots\ldots \text{(1.12)}$$

λ(0) represents penetration depth at zero kelvin[1].

1.5.2 Ginzburg-Landau Theory

The GL theory, proposed byL.D. Landau V.L. and Ginzburg in 1950, was a phenomenological theory that described superconductors quantum mechanically. The very first superconducting quantum theory had been developed.

The hypothesis begins with the assertion that a normal-superconducting conversion is a phase shift of second order without the presence of a magnetic field. Landau had developed hypothesis that specifically addressed analogous phase shifts particularly. The order parameter, which was stated in the framework, should constantly increase from zero at T_c to one at $T = 0$, in the subsequent stage (here, the superconducting phase). This implies that a superconductor has an order parameter that is nonzero order parameter at $T<T_c$ and a fading order parameter at $T> T_c$. When describing the superconducting state's order parameter, Landau and Ginzburg developed a function called $\Psi(r)$. You can interpret the number $\Psi(r)^2$ indicating the number of charge carriers in a superconducting system.

Since $\Psi(r)^2$ must reach zero consistently in the superconducting phase for $T-T_c$, we can extend the Gibbs function g_s of the superconducting state in a Taylor series of the density function $|\Psi(r)|^2$.

$$g_s = g_n + \alpha\Psi^2 + {}^1/_2\,\beta\Psi^4$$

The standard conducting phase's Gibbs function g_n occurs here, the Gibbs function g_s should be equal to g_n when Ψ=0 [10].

1.5.3. BCS theory

The Bardeen-Cooper-Schrieffer concept is a profound theory in material science that successfully describes superconductivity caused by electrons having opposite momentum and spin i.e.Cooper-pair. The interchange of virtual phonons results in an enticing attraction and, as a result, a singlet Cooper pairing [11].

1.5.3.1. Formation of Cooper pairs

Consider a free electron travelling in a crystal with wave vector k_1. It seldom causes a lattice to vibrate. In a nutshell, the electron enters an altered state termed k and produces a phonon that wasn't there before. Here q be the wave vector of a generated phonon. Hence, according to conservation principle of momentum

$$k_1 = k^{\sim} + q \text{......................} (1.13)$$

Another electron k_2, nearly instantly absorbs the phonon q, which then enters the $k_{2'}$ state. Two electrons originally occupying the k_1 and k_2 states eventually moved into the states $k_{1'}$ and $k_{2'}$.This indicates that they were scattered between themselves therefore:

$$k_1 + k_2 = k_{1'} + k_{2'} \text{.................} (1.14)$$

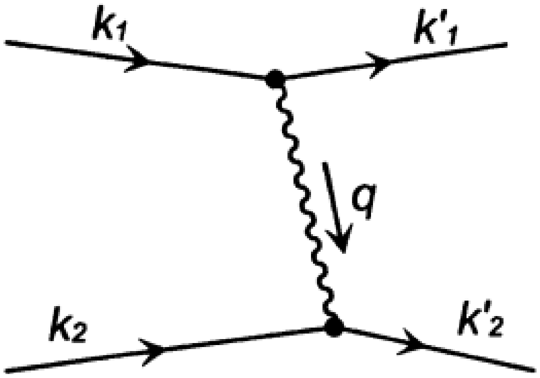

Fig 1.12: Electronelectron interaction via emission and absorption of phonon

Yet, two particles can only mutually disperse each other when they interact. As a result, we draw the conclusion that the preceding method, describes a successful electron-electron interaction. One of the electrons creates small fluctuations of the electron density at the frequency *w* as it reaches the new position $k_{1'}$ from the state k. As one of the electrons moves from state k_1 to state $k_{1'}$, it causes small fluctuations with the number of electrons at the rate of w.

Assume if at any one point in time, the regional abundance of electrons (negative charge) has increased. The neighboring ions are going to be pulled towards that point as well as will begin to flow into it, eventually compensating for an increase in density of electrons. However, due to their massive weight, the positively charged ions will continue to move despite the fact that the density increase has been rectified, resulting in an excessive charged state. Therefore, the subsequent electron with momentum $k_2$is thus going to be pulled towards it instantly, thus bringing the electrons together i.e.$k_1$along with k_2. As the outcome, the additional electron having momentum $k_2$is going to be pulled towards it quickly, bringing the particles with momentum $k_1$and k_2 together[1].

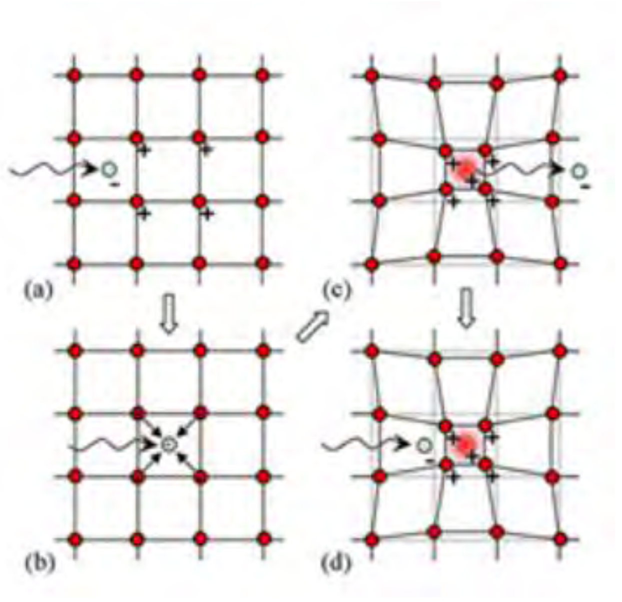

Fig 1.13: Cooper-pair formation

1.5.3.2 Coherence length

Because of the extensive range of their interaction, which could be several hundred nanometers, the electrons in a cooper pair are not always close together. They are separated from one another by a distance known as the coherence length[12].In high temperature superconductors, it is small and in case of low temperature superconductors its value is large. According to BCS theory, the coherence length is,

$$\xi = \frac{\hbar V_F}{2\Delta}$$

And 2Δ denotes energy gap while V_F refers Fermi velocity [13].

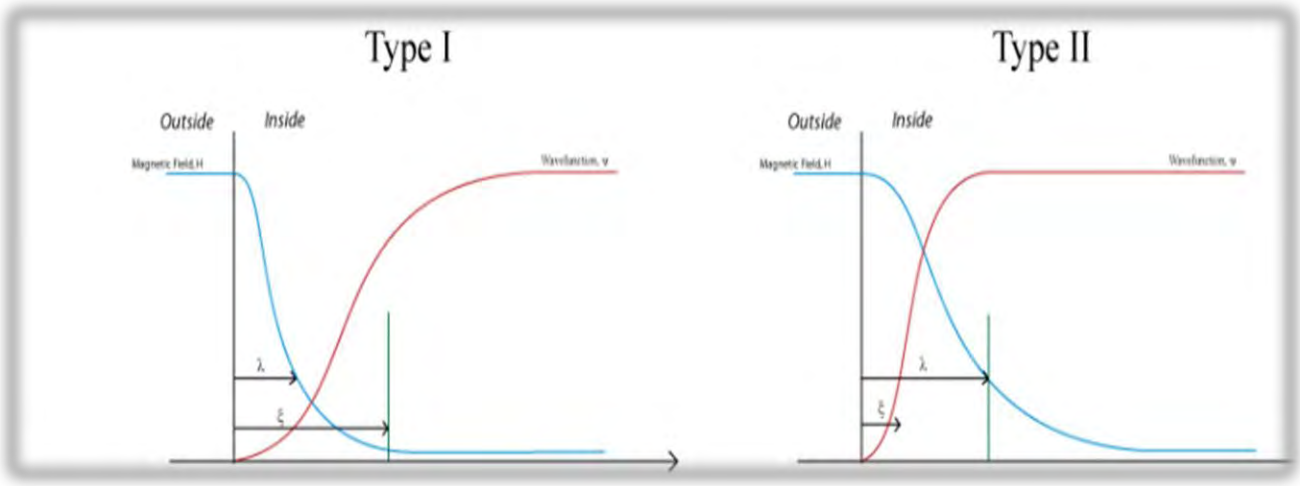

Fig 1.14: Relation regarding coherence length and penetration depth within a type 1 as well type 2 superconductor.

Superconductors of type 1: $\xi > \lambda_L$

Superconductors of type 2: $\xi < \lambda_L$

1.6 The Isotope effect

In 1950 Maxwell, Reynolds and some other scientist simultaneously identified a relation of the nuclear mass and transition temperature in mercury.

Atomic mass average	**199.5**	**200.7**	**202**	**203**
T_c(Kelvin) transition temperature	**4.161**	**4.150**	**4.143**	**4.126**

Table 1.2: *Relationship between nuclear mass and transition temperature of mercury.*

These findings were crucial to the progression in superconductivity and arrived right at the time to fully support the concept that governs the electron-phonon interaction. The effects of vibrations within the lattice are most effectively shown via isotope effect. Due to their statistical agreement with the proposed model, it supports the electron-phonon interaction's crucial significance, possibly for many superconductors. The transition temperature T_c has already been postulated by Frohlich and Bardeen to have an inverse relationship with the atomic mass square root M:$T_c \propto M^{-1/2}$

$T_c M^{1/2} = \text{constant}$

The Debye temperature of a phonon also varies inversely with mass because the mean square amplitude of vibrating lattice is inversely related to mass.

$$\theta_D M^{1/2} = \text{constant}$$

Dividing Equ. (1) by (2) gives,

$$T_c/\theta_D = \text{constant} \ldots\ldots\ldots\ldots\ldots\ldots\ldots (1.15)$$

The given statement demonstrates how crucial part lattice electron-phonon interaction and lattice vibrations play in the process of superconductivity [13].

1.7 Josephson Effect

B.D. Josephson proposed the quantum mechanical tunnelling effect in superconductors in 1962[14].He created a Josephson interconnection by sandwiching a small insulating layer among two superconductors. To allow cooper-pairs to navigate across the wall, the insulating layer ought to be thin enough i.e. of the order of 10 nm.

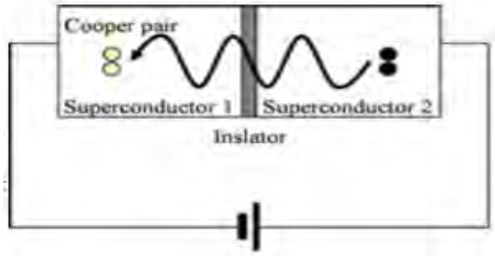

Fig 1.15: Schematic diagram of SIS tunnelling junction

The Josephson Effect is classified into two distinct kinds:

- DC Josephson Effect
- AC Josephson Effect

1.7.1.DC Josephson Effect

The estimated current stream that would flow when the Cooper-pairs penetrate through the dielectric barrier was calculated by Josephson. He discovered that under zero bias, super-current (current generated by the tunnelling of Cooper pairs) also flowed together with normal current (current generated by the tunnelling of unpaired electrons). The flow of super-current at zero bias is known as DC Josephson Effect.

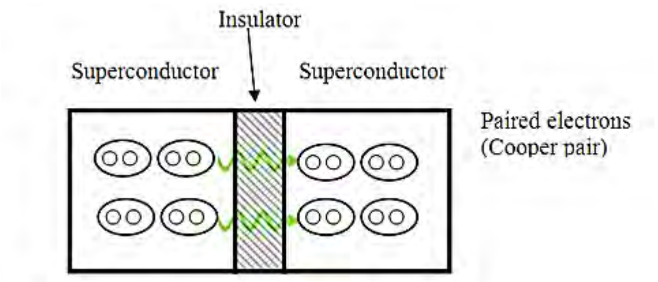

Fig 1.16: DC Josephson Effect

1.7.2. AC Josephson Effect

To create the AC Josephson effect, a constant DC power source is delivered between the junction's ends, causing a sinusoidal current to flow through the junction with a linearly increasing phase over time. The AC Josephson bridge might be described as an electrical voltage to frequency translator.

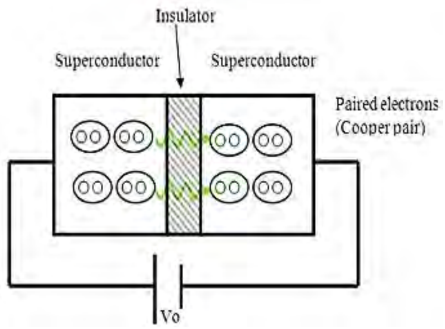

Fig 1.17: AC Josephson Effect

1.7.3. Josephson Tunneling Theory

Assume a pair of superconductors, 1 and 2, detached with the encasing obstacles, depicted in picture. For both sides the time dependent Schrödinger equation is:

$$i\hbar\frac{\partial\Psi_1}{\partial t} = H_1\Psi_1$$

$$i\hbar\frac{\partial\Psi_2}{\partial t} = H_2\Psi_2$$

Here, H_i and ψ_i correspond to the Hamiltonians and wavefunction on either side of the obstacle respectively. We hypothesized the application of a voltage of V among both of the superconductors. When a vanishing point for potential is considered to be in the middle of intersection across each of the superconductors, superconductors 1 and 2 will have a value at potential - 1/2V and +1/2V with Cooper-pair potential energy +eV and -eV respectively.

The two equations are brought together by the insulating barrier's presence:

$$i\hbar\frac{\partial\Psi_1}{\partial t} = eV\Psi_1 + K\Psi_2 \text{ .... (1.16 a)}$$

$$i\hbar\frac{\partial\Psi_2}{\partial t} = eV\Psi_2 + K\Psi_1 \text{ .... (1.16 b)}$$

Where, K≡ Coupling constant

Suppose the wave functions be defined as:

$$\Psi_1 = (n_{s1})^{1/2}e^{i\Theta 1}$$

$$\Psi_2 = (n_{s2})^{1/2}e^{i\Theta 2}$$

$$\Phi_1 = \Theta_2 - \Theta_1$$

Here n_{s1} and n_{s2} are the number densities, whereas φ is the phase difference.

Putting values of ψ_1 and ψ_2 in Eq (1.16 a) and (1.16 b) we get:

$$\hbar\frac{d}{dt}n_{s1} = 2K(n_{s1}n_{s2})^{1/2}\sin\Phi \quad \dots\dots\dots\dots\dots \ 1.17a$$

$$\hbar\frac{d}{dt}n_{s2} = -2K(n_{s1}n_{s2})^{\frac{1}{2}}\sin\Phi \dots\dots..\dots\dots\dots \text{ 1.17 b}$$

$$\frac{d\Phi}{dt} = \frac{2eV}{\hbar} \ldots\ldots\ldots\ldots\ldots\ 1.18$$

The current density can be expressed as the difference between Equ. (1.17 a) and (1.17 b) multiplied by e:

$$J = e\, {}^{d}/_{dt}\,(n_{s1} - n_{s2})$$

$$J = J_c \sin\Phi \qquad \ldots\ldots\ldots\ldots\ldots\ldots\ 1.19$$

Where,

$$J_c = \frac{4eK(n_{s1}n_{s2})^{1/2}}{\hbar}$$

Equations 1.18and 1.19 are fundamental calculations for the tunnelling behaviour of Cooper pairs which are known as Josephson relations[15].

1.8 Dielectric properties of Superconducting samples

1.8.1 Capacitor

A capacitor is a device made up of two electrical conductors separated by a dielectric material, also known as an insulator. In theory, any two conducting materials can be used to create a capacitor by encasing an insulator between them [16].

Conventional passive electrical devices known as capacitors are able to store electrical energy by rapidly polarizing dielectric materials in an electric field [17].

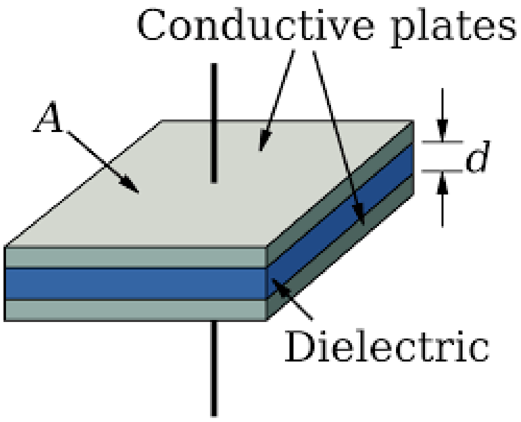

Fig 1.18: Schematic view of one typical plate-type capacitor.

1.8.2 Dielectric constant

When a capacitor is subjected to ionizing radiation or has significant electric fields applied across its thin dielectric layer, dielectric charging occurs[18]. When a dielectric substance is used to fill the space between the plates, the value of capacitance increases with an inherent proportion that is unique to that substance.

The insulator's dielectric constant between the conductors has a direct relationship with capacitance between parallel-plate capacitors.

$$C = \frac{\varepsilon A}{d}$$

Where, A≡ conductors' area and d≡ distance between conductors.

The equation for the dielectric constant,ε, is

$$\varepsilon = \frac{C_m}{C_v}$$

where $C_v$andC_m are capacitance of the vacuum and a material , accordingly[19].

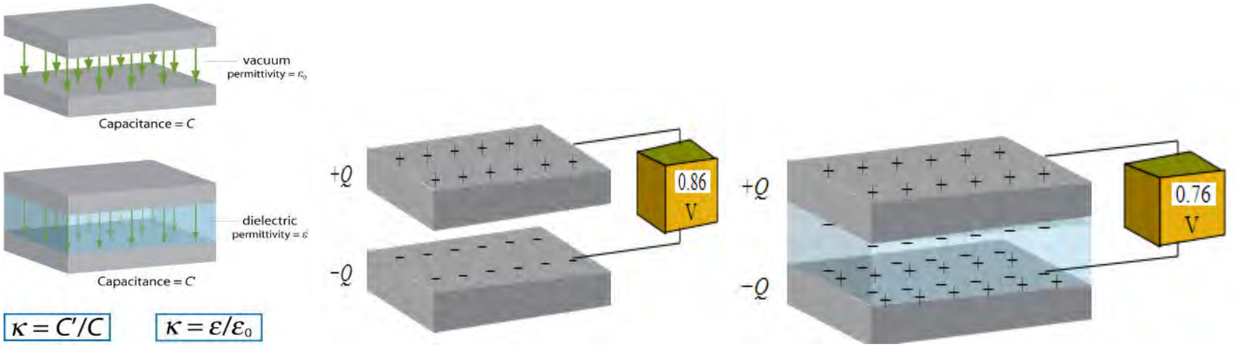

Fig 1.19: Capacitors with and without dielectric material.

As, Dielectric constant (ε) is equal to relative permittivity (ε_r) relative to the free space permittivity (ε_0.). The dielectric constant defines, the fundamental characteristics associated with a superconducting material, such as the forces that confine mobile carriers to charge reservoir layers and conducting planes. When a substance is subjected to an electrical field, its ability for preserving energy is determined by the actual part of the dielectric constant. In case of an external electric field, the hypothetical fraction of dielectric constant shows how energy is absorbed and attenuated at interfaces [20].

1.8.3 Dielectric loss

The amount of energy that is taken in by a substance during the passage of an electromagnetic wave is evaluated by the dielectric loss factor. The dissipation factor or tan delta is given by[21]:

$$\text{Tan } \delta = I_r / I_c \ldots\ldots\ldots\ldots\ldots\ldots \text{(1.20)}$$

1.9 Family of Superconductors

Cuprates are superconductors that have CuO_2 planes. Due to their high T_c (temperature above liquid nitrogen), these substances are particularly significant. The composition and fundamental characteristics of various cuprate superconductors, are essential for comprehending the mechanism of superconductivity in materials [22-23].

There are numerous series of high temperature superconductors that fall under the following categories:

- Tl-Ba-Ca-Cu-O group of superconductors
- Y-Ba-Cu-O group of superconductors
- Bi-Sr-Ca-Cu-O group of superconductors
- Hg-Ba-Ca- Cu-O group of superconductors
- Cu- Ba-Ca- Cu-O group of superconductors

Hermann and Sheng created the compound Tl-Ba-Ca-Cu-O. By varying the amount of charge reservoir layers and superconducting layers, or CuO2 planes, many different compounds can be made in this system. Such compounds are classified to Tl-2223, Tl-1114, Tl-2212 along with Tl-2201 etc. depending on their superconducting and basal planes. The last digit indicates the number of superconducting layers. $Tl_2Ba_2CuO_{6+y}$ and $Tl_2Ba_2CaCu_2O_{8+y}$are two TlO (thallium oxide) layers in certain compounds. Their T_c fluctuates between 80 and 120 K [24].

Superconductivity was also observed in $TlBa_2Ca_nCu_{n+1}$; Tl-12n(n+1) and $CuBa_2Ca_nCu_{n+1}$; Cu-12n(n+1). Although the structures are physically equivalent, however, oxygen is located differently in the charge reservoir layer. By varying oxygen atoms, which can be accomplished by adding external pressure or by substituting cations, the carrier density can be managed [25].

Superconducting characteristics of CuTl-based superconductors are closely linked to those of Cu-based superconductors. Both low and high pressures are used to create CuTl-based superconductors. In comparison with superconductors based on Tl, their anisotropy is lower and this anisotropy is brought on by the charge reservoir layer ($Cu_{1-X}Tl_xBa_2O_{4n-\delta}$) that is semi-insulating. J_c and T_c have the highest values for anisotropy γ~5 for CuTl-1223 [26].

Their greatest coherence length across c-axis, lowest superconducting anisotropy, and lack of toxicity make them among the highest-performing materials**.** Cu_{1-x} Tl_x-12(n-1) n compounds have been created by partially substituting Tl across Cu sites in charge reservoir layer in order to enhance feature and correct the deficiencies of Cu-based superconductors**.** Tl enhances the rate of reaction while also acting as a structure stabiliser. Because it is incorporated into the charge reservoir layer, it becomes easy to produce these compounds under normal pressure. In compared to the [Cu-12(n-1)n] superconductors, this hybrid group of [$Cu_{1-x}Tl_x$-12(n-1) n] materials maintains lower an isotropy and higher Tc values. Although the two families' structures are identical, the oxygen's position in the charge reservoir layer differs[27, 28].

1.9.1 Crystal Structures of (CuTl)-Ba-Ca-Cu-O Superconductors

CuO_2 planes and a charge reservoir layer make up two of the three superconducting layers in the CuTl-1223unit cell. Superconducting planes form a pyramid in the unit cell and are connected by two Ba atoms, while superconducting planes are separated by two Ca atoms. This arrangement is called p-plane. The s-plane (center plane) is the plane that lies between two p-planes. P-planes are over-doped, whereas s planes are properly doped. Charge carriers can go from the charge reservoir layer to the s-plane using p-planes as a bridge.

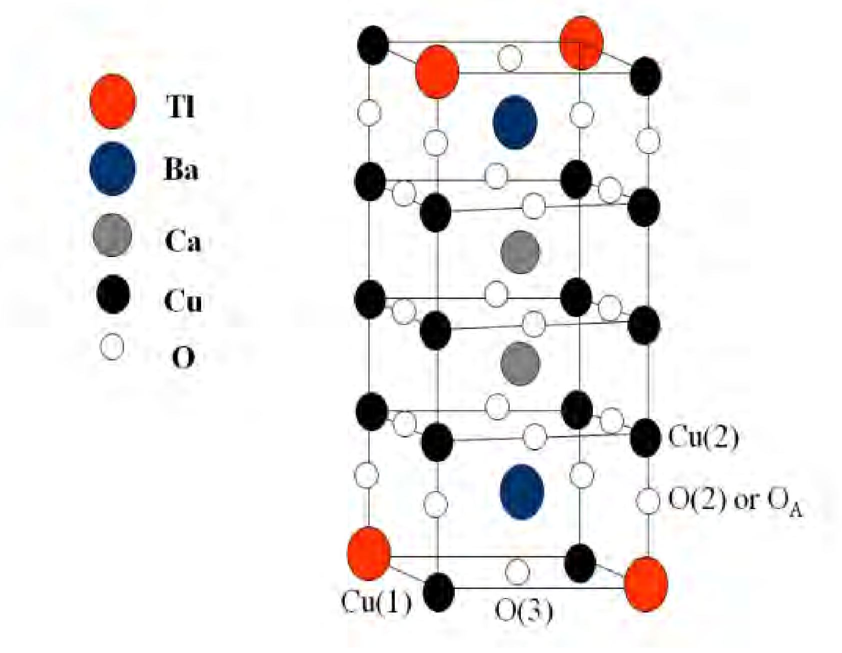

Fig. 1.20: Unit cell of $Cu_{0.5}TI_{0.5}Ba_2Ca_2Cu_3O_{12-\delta}$

The arrangement of the various atoms in the unit cell is

Cu(2) refers to the Cu atoms that are in the s-plane.

O(4) i.e. oxygen atoms in s-plane

Cu(1) i.e. Cu atoms in p-plane

O(1) i.e. O atom in p-plane

Apical oxygen, or O(2), that bridges among p-planes and the charge reservoir layer, is in charge of regulating charge transport[29].

1.10 Applications of superconductivity

Superconductivity is a game-changing field. Superconductors are extremely powerful conductors, and they are employed by engineers and scientists all over the world in research and industry. The effects of no resistance along with elevated rates of current on electrical power transportation are substantial, allowing for magnets that are significantly smaller and far stronger for:

- Power stations
- Super capacitors
- Surgical devices
- Magneto Cardiogram
- Minerals Minning

While magnetic field ejection creates a method for:

- Superconducting levitation of magnets
- Magnetic Shielding
- Magnetic Resonance Imaging (MRI): Commonly used for medical diagnosis and curing disease
- Radiofrequency imaging

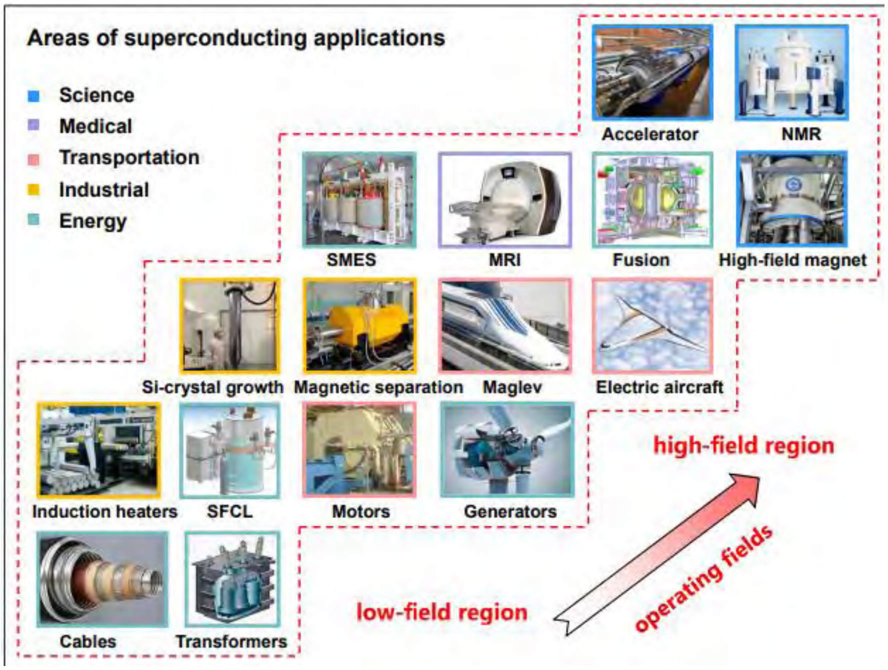

Fig 1.21: Applications of magnetic and superconducting technologies

Developments in superconductivity for electric power technology are still trying to establish a market for their products. Nowadays, there is larger requirement for powerful magnet field applications is providing a technological push to HTS drivers and will hasten their industrialization. However, experiments are ongoing to determine the market for superconducting applications in electric energy applied sciences [30].

References:

[1] V.V. Schmidt, Paul Muller and Alexey V. Ustinov, The Physics of Superconductors, (1997).

[2] R. Simon and A. Smith, Superconductors: Conquering Technology's New Frontier, Plenum, New York, (1988).

[3]Kristian Fossheim and Asle Sudboe, Superconductivity: Physics and Applications April (2004)
[4]. S. O. Pillai, Solid state physics, 5th ed
[5] Charles Kittel, Introduction to Solid State Physics, John Wiley & Sons, Inc. 8 th edition (2005)
[6] H.R. Khan, in Encyclopedia of Physical Science and Technology (Third Edition), 2003.

[7] J.E. Kunzler, E. Buehler, F.S.L. Hsu and J.H. Wernick, Physical Review Letters 6(3), 89- 91(1961).
[8] F. London and H. London, Proc. Roy. Soc A 149, 71 (1935).

[9] V.L. Ginzburg and L.D. Landau, Zh. Eksp. Teor. Fiz 20, 1064, (1950)

[10] Werner Buckel and Reinhold Kleiner,Superconductivity: Fundamentals and Applications, 2nd Edition (2004)
[11] Bennemann, K.H. Encyclopedia of Condensed Matter Physics, Superconductivity: BCS Theory (72–81) (2005)

[12]S.O.Pillai, Solid State Physics, 5th Edition, New Age International (p) Limited Publishers (2002).
[13] H. Froehlich, Physical Review, 79 (1950) 845-856.
[14] B.D. Josephson, 'Possible new effects in superconductive tunneling'', Physics Letters 1, 251 (1962).

[15] Charles P. PooleJr., ... Richard J. Creswick, in Superconductivity (Third Edition), 2014.

[16] L. Guo, T. Bashir, E. Bresky and N.-K. Persson,Smart Textiles and their Applications,Pages 657-693 (2016).

[17]Dongrui Wan and Zhi-Min Dang , Dielectric Polymer Materials for High-Density Energy Storage, 2018.

[18] De Wolf, ... S. Sangameswaran, Handbook of Mems for Wireless and Mobile Applications, 2013.

[19]James J. Licari, Dale W. Swanson, in Adhesives Technology for Electronic Applications (Second Edition), 2011.

[20] Dielectric properties of (Zn)x/CuTl-1223 nanoparticle–superconductor composite

[21] James J. Licari, Dale W. Swanson, Adhesives Technology for Electronic Applications (Second Edition), 2011.

[22] L. Gao, Y. Y. Xue, F. Chen, Q. Xiong, R. L. Meng, D. Ramirez and C. W. Chu, Phys. Rev. B 50 (1994) 4260.

[23] Andrei Mourachkine, High-Temperature Superconductivity in Cuprate, Kluwer Academic Publishers, New York, Boston, Dordrecht, London and Moscow, (2002).

[24] S.S.P. Parkin, V.Y. Lee, A.I. Nazzal, R. Sovoy, R. Beyers and S.J. La. Place, Phy. Rev. Lett. 61, 750 (1988).

[25] K. Tokiwa, H. Aota, C. Kunugi, K. Tanaka, Y. Tanaka, A. Iyo, H. Ihara and T. Watanabe, Phys. B 284, 1077 (2000).

[26] K. Tanaka, A. Iyo, Y. Tanaka, K. Tokiwa, M. Tokumoto, M. Ariyama, T. Tsukamoto, T. Wantanabe and H. Ihara, Phys. B 284, 1081 (2001).

[27] H. Ihara, K. Tokiwa, H. Ozawa, M. Hirabayashi, Akira Negishi, H. Matuhata, and Y. Seok Song, Jpn. J.Appl.Phys.33 (1994) L 503-L 506.

[28] S. K. Agarwal, A. Iyo, K. Tokiwa, Y. Tanaka, K. Tanaka, M. Tokumoto, N. Terada, T. Saya, M. Umeda, and H. Ihara, Phys. Rev. B58 9504-9509(1998).

[29] Abida Saleem and S. Tajammul Hussian, Journal of Surfaces and Interfaces of Materials 1, 1 (2013).

[30]Chao Yao and Yanwei Ma ,Superconducting materials: Challenges and opportunities for large-scale applications, 2021.

Chapter # 2

LITERATURE REVIEW

2.1 Review of High-temperature Superconductors (HTSC)

Najmul Hassan et al. created $Cu_{0.5}Ti_{0.5}Ba_{2}Ca_{0.5}M_{1.5}Cu_{1.5}Ni_{1.5}O_{10-\delta}$ (where M≡ Be, Mg) ceramic superconducting samples [1]. In order to investigate their structural and physical characteristics these samples have been generated using the solid-state reaction method. After that their FTIR analysis, resistivity assessment and ac-susceptibility measurements are carried out. The samples' XRD study found that Mg and Be addition reduced the c-axis because of their smaller atomic radii than Ca. By monitoring ac-susceptibility and resistivity after doping, a boost in the degree of T_c had been identified. A resilient inter-planar coupling was produced when elements with electronegativity that was larger than that of Ca were doped in their location. Furthermore, pairing Ni at copper regions raised the carrier concentration, which strengthened inter-planar coupling. They also marked a reduction in anisotropy and a significant rise in coherence length at the c-axis. The drop in the level of diamagnetic behaviour was due to a rise of coherence length along with a decrease in anisotropy value. By elevating dopant quantity, FTIR studies had demonstrated the softening of apical oxygen patterns.

$Cu_{0.5}Tl_{0.5}Ba_{2}Ca_{2}Cu_{3-x}Zn_{x}O_{10-\delta}$ (here, x = 0.75,1.5,2.25,2.65) materials were synthesized by N. A. Khan et al. [2] using the two-step solid-state chemical procedure while concluded that Zn alteration at the Cu planar location enhanced superconducting properties. The addition of Zn at various concentrations resulted in a shortening of the c- axis height, which was confirmed by the XRD analysis. An upward trend of resistivity was observed relative to Zn doping by means of four probe resistivity examinations. For x=2.65, a maximum T_c that can be measured is 121 K. The findings of the ac susceptibility test, demonstrating a growing pattern as Zn concentration rises, confirmed the materials' bulk diamagnetic composition. Apical oxygen phonon modes soften to a smaller number of waves for different Zn concentrations whereas the behaviour of planar oxygen modes remains steady, according to FTIR research.

In superconductors $(Cu_{0.5}Tl_{0.5})Ba_{2}(Ca_{2-y}Mg_{y})(Cu_{2.5}Cd_{0.5})O_{10-\delta}$ (y=0,0.1,0.25, 0.75, 1.0) doped with Mg, J. D. Fan et al. [3]examined roots of superconductivity. According to their explanation, the electron-phonon attraction served as a quasi-particle interaction and merely represented a particle pairing up with the opposite sign. While there is an attractive attraction among two quasi-electrons in momentum region, and there is a repelling interaction among two electrons in physical realm. Researchers discover that spontaneous superconductivity originates from the Columbic repulsive interaction.

R. Awad et al. [4]created superconducting $TlBa_2Ca_{2-x}Na_xCu_3O_{9-\delta}$ ($0\leq x\leq 0.4$) sample. Despite Tl-1223 emerging as the main phase, XRD analysis showed that multiple phases appeared in the composites. After that, they noticed the Tl-1212 phase and the $BaCuO_2$ impurity line. The "a" and "c" axes of the lattice increased after doping substance was incorporated. T_c observed to grow significantly during $x = 0$ to 0.05, but then fell once x exceeded 0.05. Furthermore, researchers emphasized as the object being examined was created within a confined vessel, the original sample became over-doped. Na atoms having a +1 valency were injected upon Ca locations to compensate up for the sample's lack of charges carriers.

When analyzing his $(Cu_{0.5}Tl_{0.5})Ba_2Ca_2Cu_3O_x$ materials around ambient temperature as well studying their influence upon critical temperature in a presence of 8 GPa pressure via a cubic anvil cell, K. Tokiwa et al. [5] reported $Tc\approx 130$ K. The CuTl-1223 superconductor reveals a single phase according to XRD analysis. They employed a four probe approach and found that at an 8 GPa pressure, the onset temperature grew by 134.6 K to 147.0 K.

The proposed infield superconducting properties of $Cu_{0.5}Tl_{0.5}Ba_2Ca_2Cu_3O_{10-\delta}$ (CuTI-1223) with nanosized Ag added was studied by M. Rabbani et al. [6] throughout a range of applied magnetic fields exceeding H=8 T. They discovered that the host CuTl-1223 had a greater flux flow and transition width, but that this flux flow decreased when nano-size Ag was added. They noted a reduction of $\xi(0)$ and an increase in $H_{c2}(0)$. They came to the conclusion that these modifications demonstrated the host CuTl-1223 superconducting phase's enhanced capacity for flux pinning.

According to Manzoor A. Malik et al. [7], A significant number of standard superconductors follow BCS phonon-mediated coupling in the conventional as well as high temperature superconductivity processes. They concluded that phonons have an important role when studying the process of traditional superconductivity.

Nawazish A. Khan et al [8] generated superconducting samples $Cu_{0.5}Tl_{0.5}Ba_2Ca_2Cu_{3-x}Ti_xO_{10-\delta}$ (where x = 0, 0.25, 0.50, 0.75). They employed their specimens around 860 °C using the solid-state reaction technique. They utilized ac-susceptibility, FTIR, x-ray, and resistivity to examine the characteristics of the samples. Using resistivity calculations, they reported that materials contained orthorhombic structures with PMMM space groups and that the T_c had been lowered by titanium doping. They determined the variables of the unit cell that had been doped with Titanium atoms at the Cu planes, the length of the c-axis and the orthorhombic deformation enhanced, resulting in that a rise in orthorhombic distortion was due to the different ionic radii, which were 0.69 Å and 0.90 Å for copper and titanium, correspondingly. According to their Fourier Transform Infrared Spectroscopy (FTIR) findings, planer oxygen modes have toughened as the amount of doping went up because they have moved towards the high wave numbers. And the larger ionic radius and smaller mass compared to the copper atom were responsible for of this hardening of planar oxygen modes. Since smaller mass atoms vibrate at greater frequencies. As a result, harmonic oscillations were generated by titanium atoms at the Cu location, which also minimized the phonon population density g(ω). As $g(\omega) = (N\tau/2\pi^2v^3)\,\omega^2$ and $\omega = qv$. Where τ indicates volume of the unit cell and N is total number of primitive cells. Since electron-phonon attraction, which must exist in superconductivity, is known to occur in CuO planes, it follows from the calculation above that if volume drops, g(ω) as well falls, which results in a reduction in phonon-electron interaction.

In their study, M. Rahim et al. [9] examined the effects regarding Be replacement upon superconducting $(Cu_{0.5}Tl_{0.5}Ba_2Ca_{2-y}Be_yCu_{2.5}Cd_{0.5})O_{10-\delta}$ (where y = 0, 0.1, 0.2 and 0.5) samples. An enhancement in T_c and T_c (onset) was discovered, most likely results from improved interplane bonding achieved through the insertion of Be across the Ca positions within the planes. However, these factors have been reduced as a result of the higher Be induction and bulkier Cd atoms located across CuO_2 planes. According to their hypothesis, the overall amount of essential phonon would be reduced by the closer spacing among the planes brought on by the incorporation of heavier Cd atoms. The vibrational apical phonon modes grew harder. They eventually came to the conclusion that an important aspect of the superconductivity process in cuprate superconductors is the electron-phonon interaction

A. Khurram et al. [10] investigated the dissipation caused by the $Tl_{1-x}C_xBa_2Ca_3Cu_4O_{12-\delta}$ superconductor found that samples with carbon concentration of x=0.25 had significant flux pinning and highly connected grains, while samples with a greater amount of carbon had lower grain morphology and weaker flux pinning.

A. A Khurram et al. [11]examined the inter-granular characteristics of superconductors $Cu_{0.5}Tl_{0.5}Ba_2Ca_{2y}Mg_yCu_3O_{10-\delta}$. A. Increased inter-plane interaction in a unit cell is due to the Mg substitution along the Ca location. In AC susceptibility tests, Mg doped materials showed increased inter-granular coupling and flux pinning. According to their observations, these samples' critical current densities increased due to greater inter-plane bindings.

$Cu_{0.5}Tl_{0.5}Ba_2Ca_{2y}Mg_yCu_{2.5}Cd_{0.5}O_{10-\delta}$ (where y =0.1, 0.25, 0.5, 0.75, 1.0) superconducting materials were synthesized by M. Rahim et al. [12]. At the Cu and Ca locations, Cd and Mg were doped. It was discovered that as Mg doping grew, the separation among the planes i.e. CuO_2/CdO_2 reduced. The occurrence of diamagnetic phenomena decreased with rising Mg concentrations. However, it was observed that apical oxygen modes were softened as a result of enhanced Mg inter-plane interaction at Ca site, whereas the phonon population was reduced caused by larger Cd atoms across CuO_2 surface, which led to a reduction in density of phonon and subsequently superconductivity. As a result, a crucial component of the superconducting mechanism of high temperature superconductors is an electron-phonon coupling.

N. A. Khan et al. [13]produced a $Cu_{0.5}Tl_{0.5}Ba_2Ca_2Cu_3O_{10-\delta}$ superconducting material by introducing Mg along with Pr across the Ca location. It was discovered that Mg doping raised critical current density by two orders of magnitude as well as improved interplane coupling. The critical temperature for zero resistance was raised by 10K, and FTIR measurements revealed a softening of the apical oxygen modes

Nawazish A. Khan et al. [14] investigated the properties of superconducting specimens $Cu_{0.5}TI_{0.5}Ba_2Ca_2Cu_{3-y}Cd_yO_{10-\delta}$ (where y= 0.5, 1.0, 1.5, 2.0) via XRD, resistivity analysis, susceptibility evaluations, and FTIR spectroscopy. X-ray scans revealed that the material was found to have a tetragonal form in the P4/mmm space category. They discovered an increase in phase stability of samples after cadmium doping. They discovered a decrease in a measure of critical temperature shortly after doping Cd atoms in the original sample through resistivity measurements. Ac-susceptibility calculations revealed a drop in diamagnetism. The decline arose due to lowering of carrier density in CdO_2/CuO_2 planes and because of the an-harmonic oscillations of large Cd atoms. FTIR scans revealed that the insertion of cadmium atoms into the location of copper atoms in the unit cell toughened apical oxygen modes while softening planar oxygen modes of phonon vibrations.

L.Perez. Arrieta et al. [15]designed their superconducting samples, $TlBa_2Ca_2Cu_3O_x$, via a two-step technique, and then they examined their behaviour. They used a two stage furnace with various thallium diffusion processes at 823K (5500C) for making the samples, and they deployed spray pyrolysis procedures to deposit the material films. Consequently, samples' precedents were created. Researchers then positioned the samples in various oxygen flow rates, inserted various amounts of thallium oxide, and built pressure to obtain the thallium oxide pressure, which ranged from $6.9 \times 10^{-}4$ to 6.1×10^{-2} atm 750°C. They therefore formed their films with the c-axis transverse to the substrate's surface. They obtained crystalline grains with broad sides and enhanced superconducting behaviour with a thallium oxide pressure of 1.4×10^{-2}atm because the samples were a blend of two materials ($BaCuO_2$ and $Tl - 1223$). The critical temperature T_c values for their films ranged from 90 K to 120 K.

2.2 Review of Potassium Doped Superconductors

N.A. Khan [16] manufactured $Cu_{0.5}Tl_{0.5}Ba_2Ca_2Cu_{3-x}K_x\ O_{10-\delta}$ (x = 0, 1, 2, 3) and $Tl_{1.0}Ba_2Ca_2\ K_3O_{10-\delta}$ samples. The XRD technique, SEM microscopy, resistivity, XRF spectra analysis, and FTIR analysis were then used to assess this superconducting material. Unit cells exhibit an orthorhombic arrangement within the P4/mmm space category, as well as a decrease in c-axis and a drop in unit cell volume upon doping, as shown by an X-ray monitoring of the specimen. They detected an increase within samples' transition temperature infused with K via resistivity experiments. The findings of FTIR analysis revealed a rightward trend in apical and planar oxygen modes, showing that the number of waves was lowered by increasing the doping agent mass that highlighted a boost in inter-planar interaction. Because K is a member of the alkali metallic class, it is able to readily lose its valence electrons, increasing inter-grain connection and minimizing voids, as evidenced by SEM pictures. Doping CRL ($TIBa_2O_{4-\delta}$) with Tl atoms instead of Cu atoms totally eliminates superconductivity of $Tl_{1.0}Ba_2Ca_2\ K_3O_{10-\delta}$ samples, resulting in semiconducting properties. A spin-bearing object must exist in the unit cell for high T_c superconductivity to manifest as well as for superconductivity to be induced in oxide samples at high temperatures.

M. Mumtaz et al. [17] investigated the function of mobile charge carriers and electron-phonon coupling in oxide HTSCs. They doped the group I-A elements (where M = Na, K and Li) in the vicinity of Tl sites of the superconductor $Cu_{0.5}Tl_{0.25}M_{0.25}$ $Ba_2Ca_2Cu_3O_{10-\delta}$ for research purposes. Shortly after doping, they discovered an improvement in superconducting properties. The charge reservoir layer retains the oxygen content of these dopants with decreased electronegativity.

Different characteristics of the $Cu_{0.5}K_{0.25}Ba_2Ca_3Cu_4O_{12}$ sample were examined by A. Younis et al [18]. Following a two-step solid state reaction process, they produced their sample, which was subsequently pelletized. They next used the mutual inductance method, the LCR meter, and the four-probe approach to characterize their sample by measuring its ac susceptibility, dielectric properties and resistivity. They claimed that the critical temperature for zero resistivity, $T_c(R=0)$, was 101 K. The sample's diamagnetic nature was discovered through susceptibility testing. Researchers discovered that the negative capacitance displayed by their sample led to negative value of the dielectric constant's real component. When the frequency and observed temperature values increased, the negative effects were suppressed probably due to a decrease in polarization density. The imaginary component in the dielectric constant dropped as frequency as well as temperature increased. They noticed a consistent increase in negative tan losses through temperature measurements, exhibiting a growing pattern indicated by increasing rate of frequency. The ac conductivity decreased with rising temperature and reached saturation at low frequencies at all temperatures measured.

K-doped few layer graphene (FLG) was created by researchers using a wet chemical method. Results from energy-dispersive X-ray spectroscopy (EDX) demonstrate that potassium was successfully intercalated into the graphene sheets. The former has a 4.5 K transition temperature and is diamagnetic. The superconducting phase is rarely removed when weak fields are used, as evidenced by the noticeable fall within χ about 4 K despite at 1000 Oe. The phenomenon of superconductivity in this substance is intrinsic since Tc is gradually lowered because of applied magnetic field. Because of potassium's extremely reactive nature, only a very little percentage of it remained in the middle of FLG nano sheets following the ethanol etching process. At 2.5 K, the M vs H curve reveals that the K-doped FLG appears to be a type-II superconductor that exhibits substantial vortex pinning. At extreme temperatures, the field cooling FC and zero field cooling (ZFC) susceptibilities correspond to the Curie Weiss temperature dependency. As a result, our findings confirm the hypothesis which suggests the measured diamagnetic indication observed in K-doped FLG is caused by superconductivity around the ideal doping level [19].

Alkali metal gas vapor and the compound C_{60} interacted inside tubes that were sealed off, whether they were under a high vacuum or under helium partial pressure. Only K-doped C_{60} turned out to exhibit a response with a superconducting transition and the maximum film conductivity. Meissner-effect measurements, microwave and resistivity are employed to prove superconductivity. A thin layer exhibited a resistance shift at an initial temperature of 16 K and almost no resistance in the vicinity of 5 K. Bulk samples showed a precise Meissner phenomenon and magnetic field-reliant microwave absorption starting at 18 K. A Meissner phenomenon and a shift to no resistance demonstrating magnetic field expulsion confirm indisputably the proof of superconductivity in K_xC_{60} [20].

2.3 Review of Excess Conductivity Analysis

The superconductors $TlBa_2(Ca_{3-y}M_y)Cu_4O_{12-\delta}$ (where y=0, 0.5, 1.0, 1.5, 2 and M=Be) were developed by Nawazish A. Khan et al. [21], who additionally implemented resistivity and ac-susceptibility tests to assess their samples. Their samples exhibit tetragonal arrangement which they explained through the method of XRD. They stated that as the percentage of doping is increased, the c-axis height shortens as the unit cell volume expands. They observed that as doping was increased, superconductivity was dropped. They carried out FTIR and noticed that the apical and planer oxygen modes were inclined towards lower wave numbers, which was a clear sign of increased interplane coupling. When they placed their samples in O_2 for annealing, the value of diamagnetism suppresses. Finally, oxygen causes the cell's carrier concentration to decrease. Consequently, superconductivity drops. Researchers confirmed that anti-ferromagnetic arrangements in the CuO_2 planes are reduced because of doped Be atoms, leading to in an increase in superconductivity. The actual objective for which they synthesized $TlBa_2(Ca_{3-y}M_y)Cu_4O_{12-\delta}$ was to improve interplane coupling and decrease anti-ferromagnetic alignment. Doping with atoms having higher electronegativity and smaller radii compared to the Ca atom can boost the inter- plane coupling. As they introduced Be atom that is smaller in size than Ca atom. It increased the interplane coupling factors and decreased the antiferromagnetic content of the CuO_2 planes.

A.l. Abou-Aly et al. developed $TI_{0.8}Hg_{0.2}Ba_2Ca_{2-x}R_xCu_3O_{9-\delta}$ (where $0 \leq x \leq 0.15$;R = Yb, Sm) material [22] whereas their characteristic thermal fluctuations appeared beyond the critical temperature. Within a range of samples at hand, (Tl, Hg)-1223 was the most pronounced phase, although an x-ray diffractometer also picked some impurities. They carried out conductivity analysis using Aslamazov-Larkin calculations and the four-probe approach for determining resistance. Following the results of this study, the crucial regime, 3D, 2D, 1D, and short wave zones of thermal fluctuations were emphasized. Conducting charge belts were present in the samples due to the 1D regime of variations present in (Tl, Hg)-1223. Sample doping reduced the coherence length while enhancing the inter-grain connectivity. Upon the insertion of the dopant, both the critical current density and magnetic field values (B_{c2},B_c,B_{c1}) dropped. Fermi energy had risen because doping caused the unit cell of superconducting samples to shrink.

Nawazish A. Khan et al. [23] researched the effect of magnesium addition on the characteristics $TIBa_2Ca_{3-y}Mg_yCu_4O_{12-\delta}$ (y = 0-2.0) of superconducting alloys adopting a para-conductivity analysis approach. The solid-state chemical reaction approach was used to create the samples, which were then annealed at 500° C. The samples' T_c(offset) and T_c(onset) values grew up to y = 1. FTIR absorption spectra demonstrated softening of apical oxygen modes along with apical oxygen modes. Excess conductivity investigation showed that enhancing Mg content in the samples increased the results in terms of inter-planar coupling J and coherence length $\xi_c(0)$ because it decreased the order parameter of charge transporters in CuO_2 planes. $B_{c1}(T)$, $B_{c0}(T)$, and $J_c(0)$ parameters went down because the injection of magnesium at calcium positions in the unit cell reduced the intensity of inter-grain interaction.

By adding chromium to the thallium and calcium sites, Annas Al Sharabi et al. [24] created $TlSr_2CaCu_2O_{7-\delta}$. According to XRD, the structure of $TlSr_2(Ca_{1-x}Cr_x)Cu_2O_{7-\delta}$ samples was Tl-1212 space group P4/mmm and tetragonal. T_c onset was between 90 and 104K. The AL model was used in the FIC study, which illustrated the transition from 2D to 3D. Anisotropy, coherence length and Josephson coupling were all calculated using the L.D. model. For sample x=0.2 greatest values of J=0.404, T2D3D=146K, and coherence length=1.011 was measured.

$Cu_{0.5}TI_{0.5-x}K_xC$-1234 (x = 0, 0.25) superconducting composites were made by M. Mumtaz et al. [25], and their higher conductivity was measured. The specimens corresponded to P4/mmm space classification and exhibited a tetragonal geometry. Charges within superconducting planes were optimized by injecting potassium ions in the charge reservoir surface, raising transition temperature of samples. Because more carriers were present in planes after annealing than was desired, the critical temperature of post-annealed K-doped materials decreased. They showed that the crossing temperatures i.e.T2D-SW and T3D-2D, and the critical temperature Tc have a direct relationship via Aslamazov-Larkin theory. The coherence length is unaffected by the charge density in CuO2 planes. They postulated that the improved dimensionality caused by moving the order parameter from the 2-D towards 3-D region led to an increase in the samples' T_c.

References:

[1] Najmul Hassan and N.A. Khan, Materials Chemistry and Physics 112(2), 412-416 (2008).

[2] N.A. Khan, M. Mumtaz, Supercond. Sci. Technol. 19 (2006) 762–766.

[3] J. D Fan, Y. M. Malozovsky, Physica C, 493 (2013) 12-14.

[4] R. Awad, A.I. Abou-Aly, S. Isber and W. Malaeb, Journal of Physics: Conference Series 43(1), 474 (2006).

[5] K. Tokiwa, H. Aota, C. Kunugi, K. Tanaka, Y. Tanaka, A. Iyo, H. Ihara, T. Watanabe, Physical Review, B 63.6 (2001) 064508.

[6] M. Rabbani, Liaqat Ali, M. Mumtaz, Iftikhar Hussain Gul, Progress in Natural Science 27 (2017) 487-490

[7] Manzoor A. Malik and Bilal A. Malik, American Journal of Condensed Matter Physics 2(2012) 67- 72.

[8] N. A. Khan and M. Arif, Physica C: Superconductivity 488 (0), (2013) 35-38.

[9] M. Rahim, Najmul Hassan, Nawazish A. Khan, Journal of Material Science Material in Electronics

[10]A. A. Khurram, Shakeel Ahmad, Nawazish A. Khan, Physica C 480 (2012) 19-22.

[11] A. A. Khurram and Nawazish A. Khan, Supercond. Sci. Technol. 19 (2006) 679-684.

[12] M. Rahim, Nawazish A. Khan, Journal of Alloys and Compounds 572 (2013) 74-78.

[13] Nawazish A. Khan, Asim Javaid, A. A. Khurram, and Naghma Haider, Physica C 425, (2005) 90

[14] Nawazish A. Khan and Asad Raza, J. Supercond Nov Magn 23, 199-204 (2010).

[15] L. Perez. Arrieta and M. Aguilar-Frutis Revista Mexicana Defisica, 54 (6)(2008) 446– 450.

[16] N. A. Khan and Anila Kanwal, Journal of electronic Materials , (2023)52: 601-612

[17] M. Mumtaz · Nawazish A. Khan · Faheem Ashraf, J Supercond Nov Magn 24 (2011)

[18]A. Younis, N.A. Khan, Mod. Phys. Lett. B 24 (2010) 3097–3107.

[19] Mianqi Xue, Genfu Chen .. and Tingbing Cao, Journal of American Chemical Society, Superconductivity in Potassium-Doped Few-Layer Graphene. 6536–6539 (2012)

[20] A.F. Hebard, M. J. Rosseinsky , .. and A.R. Kortan , Superconductivity at 18 K in potassium-doped C60, Nature, Vol 350 . 1991

[21] N. A. Khan and M. Shamraiz, Journal of Physics: Conference Series 439 (1),(2013) 012022.

[22] A.l. Abou-Aly, R. Awad, I.H. Ibrahim and W. Abdeen, Solid State Communications 149, 281 (2013).

[23] [19] Nawazish A. Khan, M. Shamraiz, S. Abbas and Azhar A. Rizvi, J Supercond Nov Magn 27, 2005 (2014).

[24] Al-Sharabi, A. and R. Abd-Shukor, Excess conductivity analysis of Cr substituted TlSr2CaCu2O7–δ superconductor at Tl and Ca sites. Journal of alloys and compounds, 2014. 615: p. 363-371.

[25] M. Mumtaz, S.M. Hasnain, A.A. Khurram and N.A. Khan, Journal of Applied Physics 109, 023906 (2011)

Chapter # 3

EXPERIMENTAL TECHNIQUES

Introduction

This section demonstrates the sample synthesis methodology and experimental techniques that have been applied to study the structural, optical, electrical, morphological, as well as dielectric characteristics of materials.

3.1 Solid-state Reaction Method

Polycrystalline ceramic superconductors are synthesized in this process using solid materials as reactants. Reaction rate is determined by structural properties, reactant surface area, and reactivity [1]. To improve the interaction between the reactants, they are first of all powdered together. Precursors are heated to high temperatures because it takes a significant amount of energy to overcome lattice energy. This temperature promotes atom mobility at a rapid rate. Although atoms move slowly within the lattice, they can move quickly by raising the temperature [2]. Calcination and sintering are the two main steps in the solid-state reaction process. Calcination is the breakdown of solid oxides into their constituent elements, which are then combined to form a new product. The sintering process improves the product's grain size and crystal structure.

3.1.1 Sample Preparation

Polycrystalline superconducting compounds were synthesized by reacting solids in two steps. $Ba(NO_3)_2$, $CaCO_3$, were used for preparing samples.

- In the first stage, we prepared a precursor for our samples by mixing and grinding $Ba(NO_3)_2$, $Ca(CO_3)$, and $Cu_2(CN)_2.H_2O$ in early measured concentrations of these compounds for one hour using a mortar and pestle, then placing this powder material in a chamber furnace (860°C) for the first 24 hours using a quartz boat. The chamber was brought to room temperature after 24 hours, and the precursor was thoroughly cooled and ground using a quartz mortar pestle. We used an alumina boat to place our sample in an 860 °C boiler for 24 hours.

- After heating, the precursors were cooled to room temperature. Then we added the appropriate measured amount of Tl_2O_3 to the precursor and ground it for another hour in the mortar for proper mixing.
- By applying 5 tons/cm^2 of pressure using a hydraulic press, pellets of this mixed precursor were created. The pellet was covered in gold foil for sintering and heated to 860 °C for 10 mints before being cooled to room temperature to produce the stable form of 1223 [3].

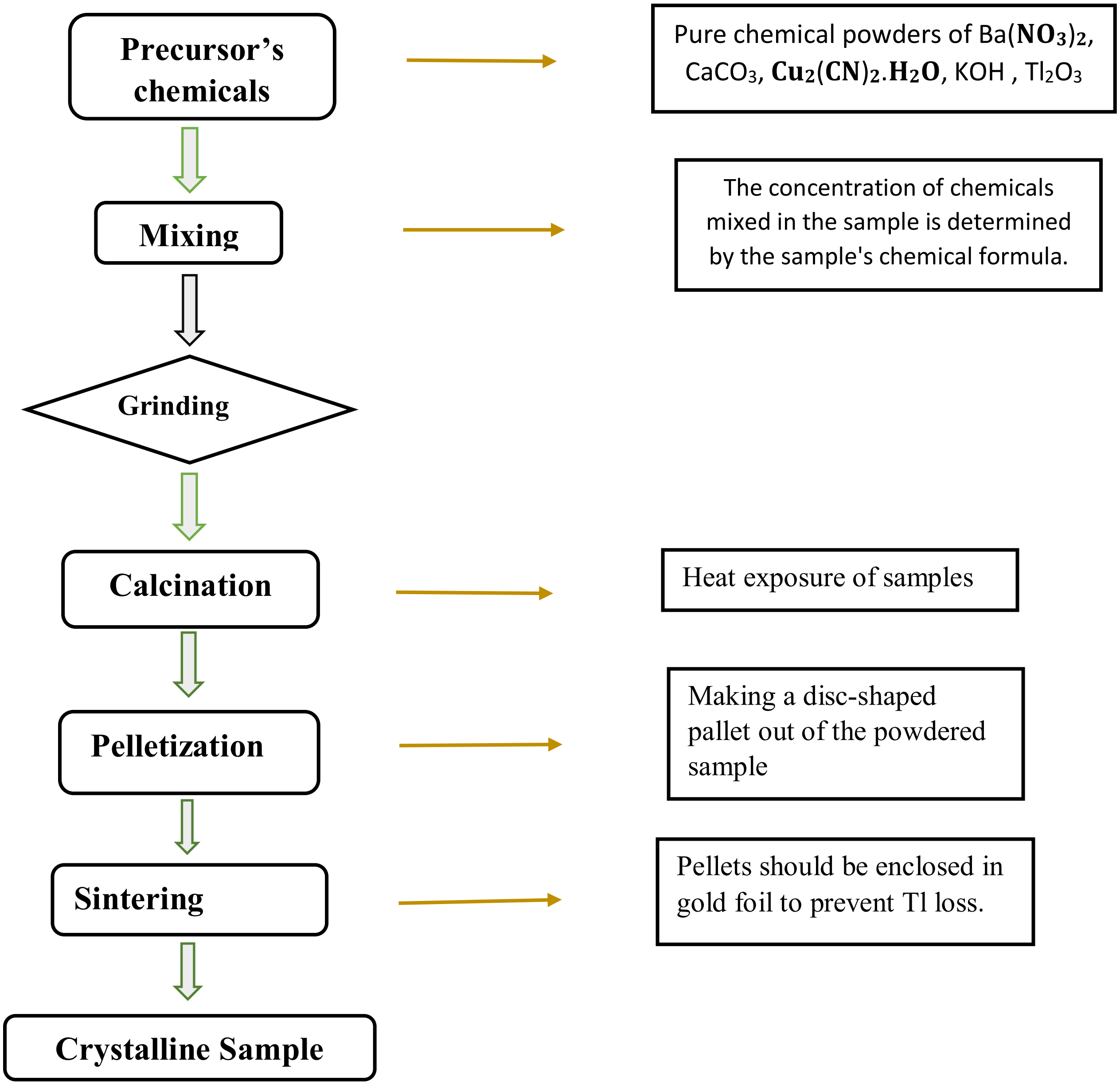

Fig 3.1: Schematic chart for synthesizing bulk superconductors

3.2 Characterization Techniques

The following illustration outlines the experimental methods used to analyse ceramic superconductors.

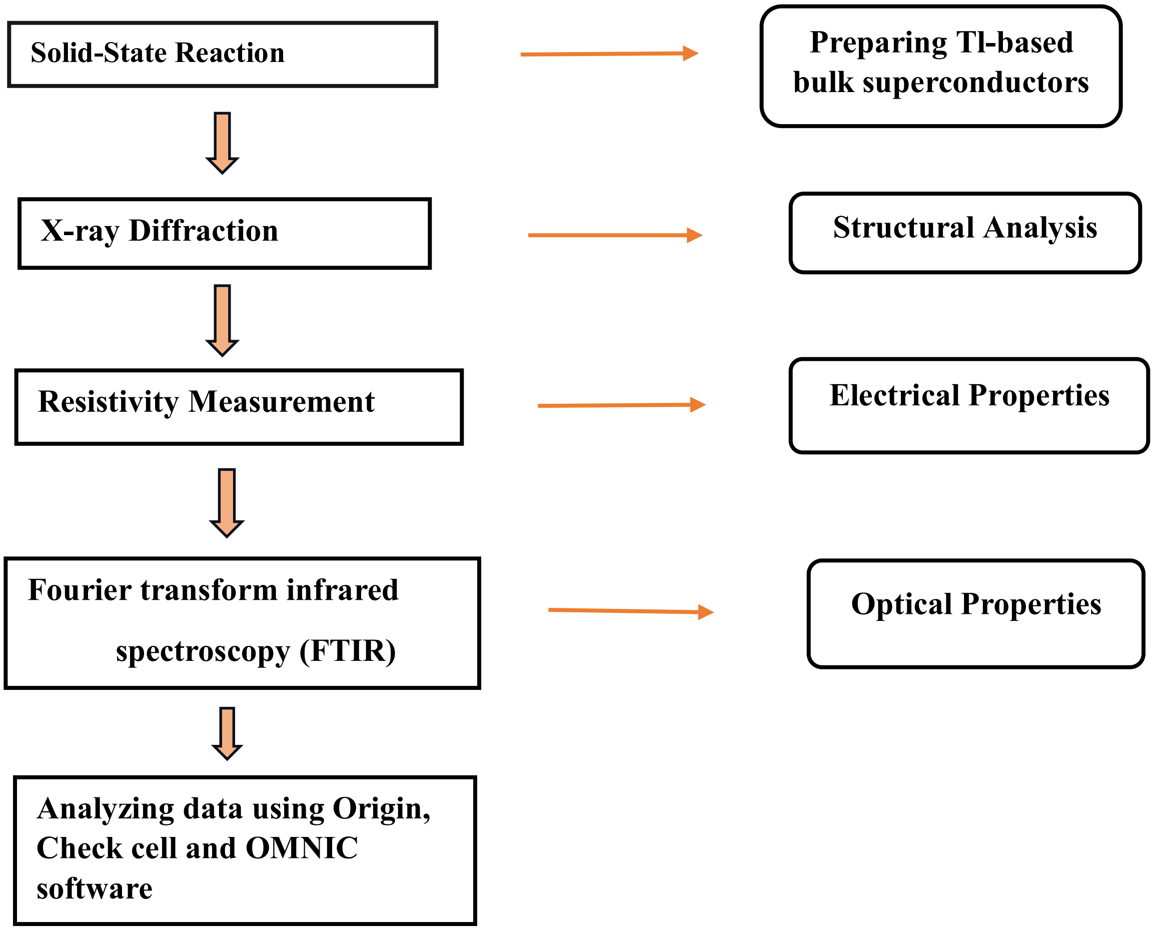

Fig 3.2: Schematic of experimental techniques

3.2.1 X-Ray Diffraction (XRD)

XRD is a method for figuring out a material's crystal structure, such as phase analysis, crystalline size lattice parameters, strain determination, stress, flaws and the identification of unknown materials. This technique employs the diffraction phenomenon, which requires that the spacing between the atoms be equivalent to the wavelength of x-rays. As the x-rays' wavelength (10 nm) meets criteria so x-rays are employed to analyze crystal structure. Cu or Mo is typically utilized to generate x-rays having wavelengths of 0.8Å and 1.54Å, correspondingly [4,5]. Bragg was the first to suggest X-ray diffraction through crystalline material [6].

3.2.1.1 X-ray Photon Energy

X-ray photon has an energy of,

$$E = h\vartheta$$

or $$E = hc/\lambda$$

If λ =0.0998nm, as hc= 1240 eV.nm

$$E = 12.42 \text{ Kev}$$

To analyze the crystalline structure of materials, X-rays should be in the 10KeV to 50KeV range. X-ray photons with this energy (10KeV to 100KeV) can penetrate below the layer of a crystal and form the foundation for many standard methods for investigating unknown 3D structures [7].

3.2.1.2 Basic working principle of XRD

XRD is based on Bragg's law. It was first proposed by a father-son collaboration (Lawrence and Henry Bragg). They identified a specific angle of reflection of x-rays from crystalline materials. High-energy electromagnetic waves with a small wavelength are referred to as X-rays. Consider two monochromatic x-ray beams are incident on a crystal with d interplanar space. Suppose it is incident at an angle. The crystal reflects both beams at the same angle. By creating the perpendiculars A_1B and A_1C, one can determine the path difference between the two beams.

$$\text{Path difference} = BA_2 + A_2C$$

$$BA_2 = A_2C = d\sin\theta$$

$$\text{Path difference} = 2d\sin\theta$$

The path difference between two reflected waves must be an integral multiple of their wavelengths in order for constructive interference to occur. The following is the criterion for constructive interference:

$$2d\sin\theta = n\lambda$$

Where ‘n’ is a positive integer. Equation is a well-known Bragg's equation that can be applied to calculate d if the wavelength of x-rays is specified. The use of Bragg's law to analyze crystal structure created the groundwork for x-ray crystallography [8].

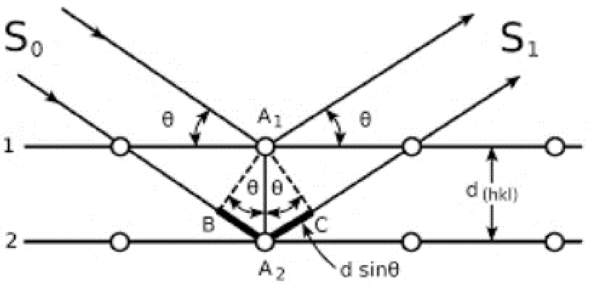

Fig 3.3: X-rays diffraction from crystal planes

3.2.1.3 X-ray Diffractometer

Materials are bombarded by x-rays in an x-ray diffractometer, which interact with them and create a scattering pattern that assists in determining the crystal structure. An x-ray diffractometer consists of the following parts:

- X-ray Generator
- Specimen holder
- X-ray Monitor

Cathodes generate x-rays and then filtered to produce monochromatic radiation [9].

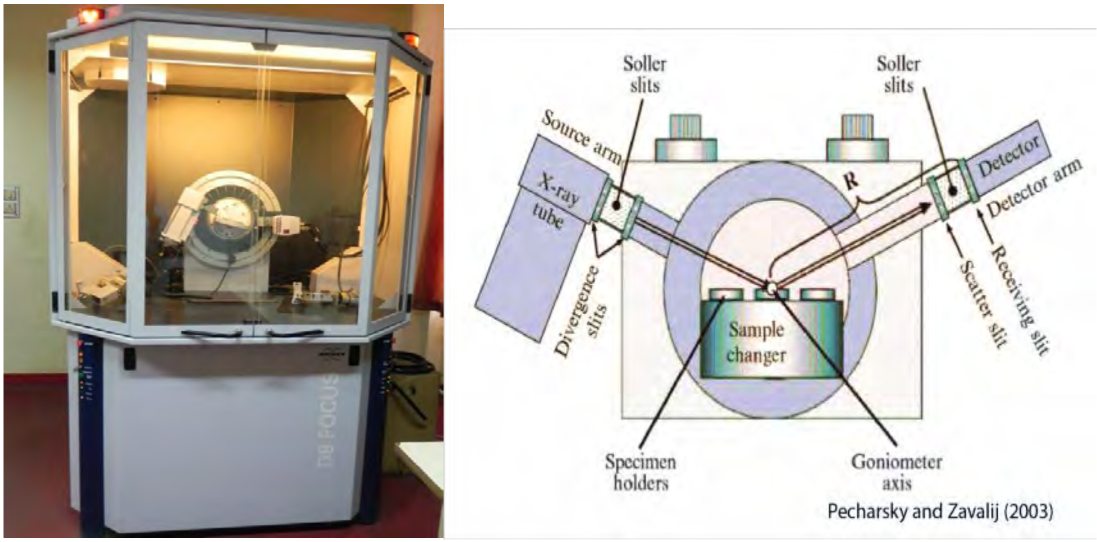

Pecharsky and Zavalij (2003)

Fig 3.4:(a) X-rays diffractometer (Bruker D8 focus) (b) Inset of the X-Ray diffractometer

A sample is maintained by a smooth plate in a way that allows it to rotate around an axis perpendicular to the paper's surface. By channeling the rays from a slit within an X-ray tube, monochromatic X-rays are created. When the beam strikes the specimen, diffraction occurs. The magnitude of diffracted rays is calculated using a counter. On the same plane specimen, counter, and x-ray source are located. The counter has a rotational axis and its angular displacement is given by 2θ. The sample and counter are positioned so that if a sample is moved by an angle, the counter will move by an angle as well, producing a corresponding angle of incidence and reflection.A function of 2θ is used to record the intensity of the diffracted rays.

3.2.1.4 Structural analysis of samples

- The detector measures the reflected x-ray photons from the crystal and displays them as a pattern on a computer screen using a computer program. This pattern's comparison with the reference pattern helps in establishing the crystal structure. The lattice parameters are determined using the "Checkcell" software**.**
- The crystalline or amorphous nature of the crystal structure is confirmed via X-ray diffraction studies. If there are more sharp intensity peaks, the structure is crystalline; otherwise, it is amorphous [10].

3.2.2 Evaluation of Resistivity

Conductors, insulators, and semi-conductors can be classified according to the band gap that exists between their valence and conduction bands. In contrast to semiconductors, insulators have a wide band gap between their valence and conduction bands. However, conductors have overlapping valence and conduction bands. The application of a potential difference between the ends of a wire permits electrons to pass across the valence towards the conduction band. Drude model gave following expression for the resistivity of electrons caused by collisions with lattice atoms as:

$$\rho = \frac{m}{n\tau e^2}$$

Where, m≡ mass of an electron, e≡ electronic charge,τ≡mean free time for the collision of two electrons, e≡ electronic charge and n≡ electron′s number density.

3.2.2.1 Dependence of resistance on mean free time

Due to an equal distribution of ions and electrons within it, metal is neutral at equilibrium. In response to an external electric field, electrons that are free begin to move through metal, causing current to flow through it. Ions do not scatter electrons at T=0 because they are regularly distributed in the lattice, but impurities and dislocations inside the crystal lattice are responsible. Because real metals contain impurities and lattice irregularities, they prevent electron flow even at low temperatures. The resistivity due to lattice defects at T=0 is known as residual resistivity $'\rho_i$. As the temperature rises, thermal vibrations start to occur in the lattice atoms. These lattice vibrations also produce phonon resistivity, or $'\rho_{ph}'$ which is a resistance to the flow of electrons [11]. Hence, the electrical resistance is dependent on mean free time due to:

- Electron dispersion from lattice defects, or impurities.
- Electron scattering from thermal lattice vibrations, or phonon-induced scattering.

The total probability of scattering of electrons is written as:

$$\frac{1}{\tau} = \frac{1}{\tau_i} + \frac{1}{\tau_{ph}}$$

As a result, resistivity is stated as:

$$\rho = \rho_i + \rho_{ph}$$

3.2.2.2 Dependence of resistance on temperature

The amplitude of lattice vibrations increases with temperature, and this rise in amplitude enhances the collisions between electrons and lattice vibrations (phonons), which in turn causes the resistivity to increase. At low temperatures, however, these collisions decrease, as does resistivity. Experimental evidence for alkali metals shows that resistivity is temperature dependent [12]. Resistivity at high temperatures is proportional to the mean square amplitude of phonons.

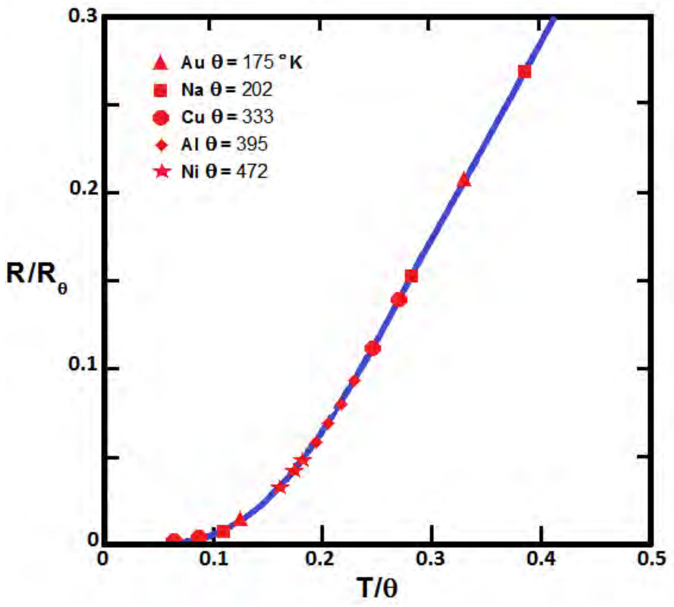

Fig. 3.5: The phonon contribution to the resistivity in normal metals.

3.2.2.3 Dc-resistivity

According to Ohm's Law, the potential difference applied at the terminals of a conductor is proportional to the flow of electric current through conductor.

$$V \alpha I$$

$$R = {}^{V}\!/_{I}$$

Hence, resistance varies with length and is inversely proportional to cross-sectional area.

$$R \propto \frac{L}{A}$$

$$R \propto \rho \frac{L}{A}$$

The resistance in the preceding statement varies with temperature.

$$\rho(T) \propto R(T) \frac{A}{L}$$

Put value of resistivity equals:

$$\rho(T) = \frac{VA}{IL}$$

The resistivity is measured in units of Ω-m if the following values are used: area 'A' in m^2, length 'L' in m, current 'A' in amperes, and voltage 'V' in volts.

3.2.3 Four-probe Method

Using the four-probe approach, the resistivity of metals, semiconductors, and superconductors is determined. It is preferable to the two-probe method because the latter method introduces error due mainly to lead contact resistance [13]. The two-probe approach only measures resistivity up to -m, but the four-probe method measures resistivity up to milli or micro Ω-m. The four-probe method involves making four equidistant contacts with the surface of a flat superconducting sample using silver paste. Silver paste produces high-quality contacts that do not break even when the sample is cooled to extremely low temperatures. The two outer contacts allow current to flow from the superconducting surface, while the two inner contacts allow voltage to pass through the sample.

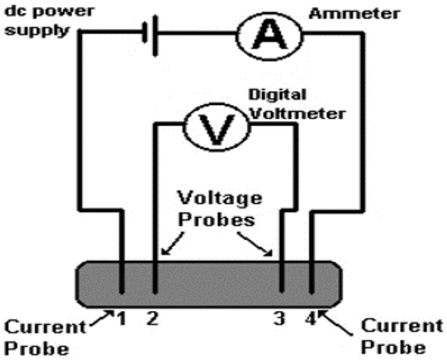

Fig3.6: Schematic of four-point probe

We have used a 1 mA current to measure resistivity using this method. Since superconductivity occurs at temperatures below room temperature, liquid nitrogen is utilised to chill samples. The resistivity of the sample can be found by using the relation:

$$\rho(T) = \frac{VA}{IL}$$

The following are the steps for measuring with the four-probe method:

- A simple cryostat was filled with liquid nitrogen, and a brass sample holder was attached with sample on one end and wires on the other.
- As a continuous current source, a MW2122A regulated DC electric generator was wired in series with the resistance.
- The change in voltage caused by temperature variation was measured using a P-2000/E KEITHLEY MULTIMETER.
- The thermocouple recorded temperature in millivolts.

• The current was measured with an ammeter connected in series with the resistance up to 1000 A with a minimum count of 1 A [14].

3.2.4 Fourier Transform Infrared Spectroscopy (FTIR)

FTIR serves a purpose for determining and evaluating unidentified compounds, determining contaminants within the material, spotting additives, diagnosing decomposition as well as oxidation via scanning samples with infrared light.The alteration of the regular pattern of absorption bands clearly demonstrate the change in specimen structure.

3.2.4.1 Elements of FTIR

The components of a typical FTIR spectrometer are:

- Infrared Radiation Source
- Specimen cell
- Monitor
- An A/D converter
- Amplifier
- Michelson interferometer.

3.2.4.2 Basic Mechanism

Radiation from the sources reaches the detector after passing through the interferometer. Since Michelson interferometer plays a crucial role in FTIR spectroscopy. Lets look how Michelson interferometer works.

The Michelson Interferometer:

- The Michelson interferometer consists of the two mirrors M1 and M2, which are arranged as shown in Figure.

- The Michelson interferometer is made up of two mirrors, M1 and M2, which are positioned as illustrated in Figure , along with a beam splitter positioned 45 degrees from the mirrors.
- When a collimated laser light beam contacts partially reflecting surface of the beamsplitter, it is split into two beams.
- Some of the light travels to mirror M1, is reflected by M1, and then returns to the beamsplitter. The semitransparent beam splitter will reflect a portion of this light.
- In order to superimpose the first light ray, a second light ray first travels through the beam splitter towards mirror M2, is bounced back towards beam splitter, and it will reflect some portion of this light.

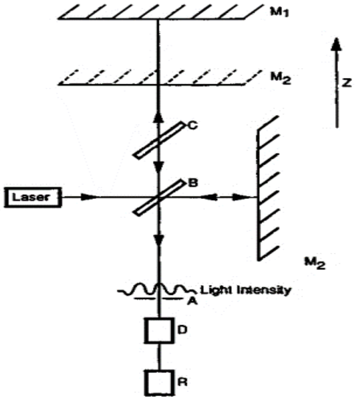

Fig 3.7: Michelson Interferometer

- The phase difference arises due to the translation of moving mirror results in the formation of the interference pattern on the recombination of these beams.
- Both beams only contain just a fraction of the original light; the rest of light had been lost at the beam splitter due to reflection or transmission and was then reflected back towards the detector.
- The A/D converter and amplifier improve the signal, which is subsequently converted to a digital signal.
- • The Fourier transform is then carried out by the computer after the signal has been transferred there [15].

Fig 3.8: Thermo Nicolet 5700, Fourier Transform Infrared Spectrometer (FTIR)

3.2.4.3 Experimental procedure for FTIR Spectroscopy

The experimental procedure for analyzing vibrational modes of polycrystalline ceramic superconductors using Nicolet 5700 FTIR spectrometer is given below:

- For the superconducting samples, the spectrometer's range was adjusted at 400 cm-1 to 700 cm-1, with 200 scans conducted to take the spectrum.
- Then, KBr pellets were created, and the spectrum of those pellets was set as the backdrop spectrum.
- Superconducting sample and KBr were combined in the proper proportions, stirred for two to three minutes, and then pelletized. After that, the pellet was placed in a sample holder so that the absorption spectrum could be taken.
- We obtained the spectrum of our sample after subtracting the baseline KBr spectrum.
- The OMNIC programme was then used to examine that absorption spectra [16].

3.2.5 Fluctuation induced conductivity analysis (FIC)

Fluctuation induced conductivity analysis, also known as "para conductivity analysis," is a method for examining superconducting variations caused by the creation and destruction of Cooper pairs down to the onset temperature. Cooper pairs begin to form above the transition temperature, but thermal turbulence causes them to continue forming and annihilating until Tc(R=0). Due to creation and destruction of cooper pairs, superconductor fluctuates. When we cooled our sample below Tc(R=0), the density of fluctuation decreased, demonstrating that thermodynamic fluctuation was ineffective in preventing the formation of a cooper pair. Zero resistance was produced as a result of the cooper pairs condensation [17].

The temperature regime around Tc, also known as the Ginzburg criterion temperature (TG), is where these variations in induced conductivity are observed. TG is less than 1 K for low temperature superconductors and between 1-2 K for high temperature superconductors. As a result, these variations may be examined. Ginzburg was the first scientist to explore how heat capacity fluctuations function and to determine the temperature value at which fluctuation adjustment to heat capacity is critical, as demonstrated by the relationship below.

$$\frac{\Delta T}{T_c} \sim \left[\frac{(T_c)^4}{\varepsilon_f}\right] \sim \left[\frac{(\alpha)^4}{\xi}\right] \sim 10^{-4} \text{ to } 10^{-16}$$

In this case, "a" denotes the interatomic separation between two lattice sites while "ξ" denotes the coherence length. These modifications have gone unnoticed in experiments for a very long time because T/T_c has such a small value. As a result of the fluctuation that led conductivity to notably vary from its linear dependency at higher temperatures, given as

$$\Delta\sigma(T) = \frac{\rho_n(T)\text{-}\rho(T)}{\rho_n(T)\rho(T)}$$

Here, the projected resistivity for the normal state is provided by $\rho_n(T) = \alpha + \beta T$ whereas the real resistivity is denoted by ρ(T). Usually, two different types of fluctuation are referred to as Δσ(T). The Aslamazov-Larkin (AL) contribution, which results from an excess current brought on by Cooper pair fluctuations at temperatures higher than T_c [18].

The second one, by Maki- Thompson (MT), discussed how the conductivity of standard electrons was affected by superconducting carrier oscillations. An alternative model, known as the Lawrence-Doniach (LD) model, shows the crossover point between a three-dimensional (3D) electronic state and a two-dimensional (2D) electronic state. For moderate pair breaking, the MT term has a strong impact in the 2D fluctuation area, whereas the AL term is dependent on phase-relaxation time tφ and is found close to T_c [19].

Many academics supported the study of crossover temperatures using the LD model, however due to the MT contribution's limited capacity to evaluate, few academics were persuaded. Although the results differ slightly from thin films, FIC analysis of polycrystalline bulk material is generally comparable with the 3D fluctuation feature. In thin films with considerable c-axis orientation, 3D to 2D crossover has been observed. The temperature range influences how effectively 3D fluctuations or 2D-3D crossover work. Various experimental results for a single crystal have been discovered [20].

3.2.6 Scanning Electron Microscope

An electron microscope called a scanning electron microscope (SEM) assesses a sample's surface to produce graphic images. It performs this by directing an electron beam at it. A number of signals are produced when electrons come into interaction with atoms within a sample, providing the details of the surface topography and chemical composition of the sample. SEM is based on a centered stream of electrons that scans the object and interacts with the atoms in the sample to yield three-dimensional surface topography. Specimens are often observed in a conventional SEM under vacuum conditions and varying pressure, and some SEMs exhibit resolutions higher than a nanometer [21].

A highly concentrated and focused electron beam is created when electrons generated at the upper part of the a section are accelerated downward and flow through an array of lenses and apertures.Under vacuum, a sample mounted upon a mobile plate is hit by the electron beam on its surface.Moving electron-beam coils scans the sample surface. The details about a particular region of the sample is provided by the resulting beam scanning technique.Numerous signals are produced as a result of the electron beam's contact with the sample and can then be picked up by the right detectors.

Components of SEM:

Electron source, electromagnetic lenses for focusing electrons, electron detection devices, specimen chambers and displays for viewing the pictures.

Working Principle:

SEM is consisting of an electron generator that directs an electron beam at the object under examination.

The beam travels via two magnet-powered lenses that can bend electron pathways.

By focusing and controlling the electron beam, the lenses make sure that the electrons are directed towards the specimen.

Vibrations don't occur in the stable, sample chamber. Additionally, the specimen is moved about and positioned at different angles in the sample chambers.

Multiple detectors are utilised by SEM to provide:

(1) the finest representations of an object's surface and

(2) show the structure of a material.

The crucial factor is that a vacuum is necessary for SEMs to operate. Surface changes would occur due to the dispersed electron beam if there was no vacuum.

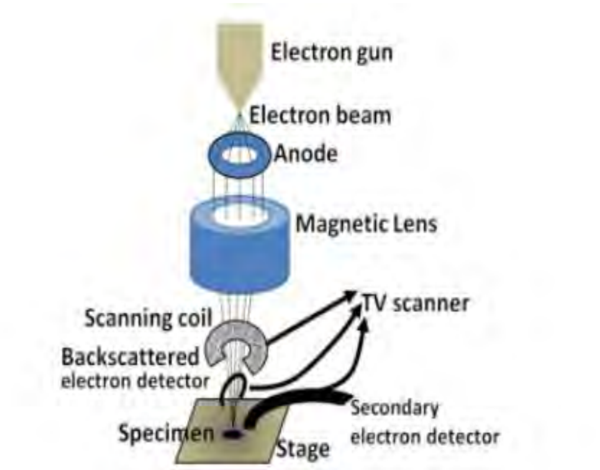

Fig 3.9: Schematic diagram of SEM

Advantages and disadvantages of SEM:

SEM has the ability to image topography in three dimensions (3D) in great detail and provides a variety of information from its various detectors. Both the accompanying software and the microscope are facile to use. The size and cost of SEM are some of its drawbacks. SEM is also cost-prohibitive to run. One significant disadvantage is that solid and inorganic substances must be sufficiently small for placement within a vacuum chamber with a low vacuum pressure in order to be studied using SEM [22].

References

[1] M. Paulus and P. Hagen Muller, Preparative methods in Solid State Chemistry, Academic Press, New York, 487 (1972).

[2] I. Parkin, Chemical Society Reviews 25(3), 199 (1996).

[3] J.S. Blakemore, Solid State Physics, Cambridge University Press, (1985).

[4] B.D. Cullity, Elements of DIFFRACTION, 2nd Edit, Addision-Wesely Publishing Company, Inc. London, (1977).

[5] M.A. Omer, Elementary Solid State Physics, First Edit, Wesely Publishing Company (1974).

[6] Thomsen, John S, A. F. Burr, American J Phy 36.9 (1968) 803-810

[7] Bragg W.H; Bragg W.L, Proc. R.: Soc. Lond,88(1913)428-438.

[8] W.H. Bragg and W.L. Bragg, Proc. R. Soc. Lond. A 88, 428 (1913).

[9] B.E. Warren, X-ray Diffraction, Dover Publications, (1969).

[10] A Simplified Approach to the Solid State Physics, M.N Rudden, A.Inst. P.J. Wilson, (1971)

[11] M.N. Rudden and J. Wilson, Elements of Solid State Physics, 2nd edition (1993).

[12] K.L. Horouitz and V.A. Johnson, Academic Press, New York and London, 401 (1959).

[13] N.W. Ashcroft and N.D. Mermin, Solid State Physics, World Publishing Corporation, (1976).

[14] P. Griffiths and J.A. De Haseth, Fourier Transform Infrared Spectroscopy, 2nd edition, Willey, New York (2007).

[15] John F Ready, Industrial Application Of Lasers, Second Edition, 249-251 (1978)

[16] S. Cavdar, H. Koralay, N. Tugluoglu and A. Gunen, Supercond. Sci. Technol. 18, 1204 (2005).

[17] Khan, N.A. and M. Mumtaz, A new $Cu_{0.5}Tl_{0.5}Ba_2Ca_2Cu_{3-y}Zn_yO_{10-\delta}$ high-temperature superconductor with three ZnO_2 planes. Superconductor Science and Technology, 2006. 19(8): p. 762-766.

[18] L. G. Aslamazov, A. L. Larkin, Phys. Lett. A 26 (1968) 238.

[19] M. Muzaffar, M. Usman, N. A. Khan, Int J Mod Phys B 30.18 (2016) 1650112.

[20] S.J. Hagen, Z.Z. Wang, N.P. Ong, Phys. Rev. B 37.13 (1988) 7928

[21] Stokes, Debbie J. (2008). Principles and Practice of Variable Pressure Environmental Scanning Electron Microscopy (VP-ESEM). Chichester: John Wiley & Sons.

[22] Ashok K. Singh, Engineered Nanoparticles ; Structure, Properties and Mechanisms of Toxicity ,125170 (2016).

Chapter #4

RESULTS AND DISCUSSION

4.1 Introduction

The discovery of high-temperature superconductors has opened an entirely new field of research and development in materials science [1]. When specific materials were discovered to show superconductivity at temperatures greater than the previously accepted limits. This discovery has important ramifications for physics, engineering, and energy transmission, among other topics. It has the potential to completely alter technology like magnetic resonance imaging, energy storage, and power generation. To fully realize the potential of high-temperature superconductors, scientists are still investigating their characteristics and uses in daily life [2,3]. Most high-temperature superconductors with the highest critical temperature are cuprates with perovskite structures [4]. The Tl-Ba-Ca-Cu-O family of superconductors is one of the most significant families of high-temperature superconductors[5]. The Tl-Ba-Ca-Cu-O superconductor consists of a tetragonal or orthorhombic structure composed of two-dimensional copper-oxide layers and a carrier supplying charge reservoir layers (CRL) ($Cu_{1/2}Tl_{1/2}Ba_2O_{4-\delta}$) that provides electrons to the copper oxide (CuO_2) planes due to their higher Fermi level [6]. The $Cu_{1/2}Tl_{1/2}Ba_2Ca_2Cu_3O_{10-\delta}$ (CuTl-1223) superconductors have three conducting CuO_2 planes sandwiched between two charge reservoir layers. The charge reservoir layers (CRL) ($Cu_{1/2}Tl_{1/2}Ba_2O_{4-\delta}$) have a higher Fermi level than CuO_2 conducting planes. As a result, CRL provides carriers to the conducting planes, which subsequently act as a source of superconductivity in these low-dimensional systems; superconductivity is affected by the carrier density of superconducting conducting planes.[7,8]. In the center of the CuO_2 planes lies the Calcium atom in the body-centered position. Calcium atoms actually separates two CuO_2 superconducting planes [9] and develop a correlation in their coherent movement in various conducting planes. The charge reservoir layer is approximately 4.2 Å thick, whereas the thickness of superconductor blocks with calcium atoms between them is roughly 3.2 Å[10,11]. The most common methods for adjusting these parameters is pressure or chemical doping [12-14]. The effect of copper oxide planes on the structural and superconducting properties in all Tl-Ba-Ca-Cu-O phases were extensively studied by our group [15-17]. For example the Calcium atom was replaced by Titanium at the interplaner sites in the unit cell of $(Cu_{0.5}Tl_{0.5})Ba_2(Ca_{2-x}Ti_x)$ $Cu_3O_{10-\delta}$ (x = 0, 0.25, 0.50, 0.75, 1.0) superconductors [18]. Ti has smaller ionic radii (0.9 Å) in comparison to Ca (0.99 Å) and higher electronegativity it lead to strong interplane coupling and enhanced the superconductivity in the final compound. Our group have also investigated the impact of adding Be, Sr, and Mg dopants to the Ca sites on interplane coupling. These elements were partially doped at the Ca sites, which reduced the length of the c-axes and increased the critical temperature and strength of the diamagnetism of these compounds. Theseexperiments led us to the conclusion that raising the inter-plane increases the superconducting of these substances [19-21]. To investigate any significance of spin density in high temperature superconductivity. The alkali metals like potassium are well known for their capacity to emit electrons. The Potassium atom was replaced by the copper atom in the CRL to give $(Cu_{0.5}Tl_{0.5})Ba_2Ca_2Cu_{3-x}K_xO_{10-\delta}$($x$ = 0, 1, 2, 2.5, 3) superconducting samples [22]. All samples demonstrated free carrier doping in the conducting planes, which changed the material with conducting CuO_2 planes into the over-doped regime of the free carriers and thus encouraged superconductivity. This encourages us to use other methods to better investigate the impact of potassium doping.

To further elaborate on the importance of Potassium in such compounds we have doped Potassium at the Calcium sites by synthesizing $(Cu_{1/2}Tl_{1/2})Ba_2(Ca_{2-x}K_x)Cu_3O_{10-\delta}$(x=0, 0.5, 1, 1.5) samples. However, compared to Ca (40.07 amu), K has a lesser atomic mass (39.098 amu). Due to the difference in masses between K and Ca, it is anticipated that the K atoms being doped will effect the interplanar coupling that will suppress the required phonon density and help to understand the function of atomic mass (electron-phononinteraction) in the mechanism of high temperature superconductivity.The X-ray diffraction, four-probe resistivity, scanning electron microscopy (SEM), and the FTIR absorption measurements were then used to characterize these materials. Furthermore, excess conductivity analysis was used to study the impact of doped K atoms.

4.2 Experimental

The two-step solid-state reaction technique was used to synthesize the samples of CuTl-1223 doped with potassium. Calculated amount of KOH(Sigma-Aldrich, 99.9% pure),$Ba(NO_3)_2$ (ACS reagent Sigma-Aldrich, 99% pure),$Ca(NO_3)_2$(Sigma-

Aldrich, 99% pure), and CuCN (Sigma-Aldrich, 99% pure) werechosenas the startingcompounds.The chemicals were properly weighed and measured before being crushed in a mortar pestle for 30 minutes. The blended powder is then ignited in a quartz boat for a day (24 hours) at 880°C. [14,15,21,22]. The fired material is then again grounded in a mortar pestle and fired for another day at 880°C but this time in an alumina crucible. In the next step,the fired material was mixed with the calculated amount of Tl_2O_3(Sigma-Aldrich, 99% pure) to give $(Cu_{1/2}Tl_{1/2})Ba_2(Ca_{2-x}K_x)Cu_3O_{10-\delta}$(x=0, 0.5, 1, 1.5) as a final reactant composition and palletized under the pressure of 3.8 tons.cm^{-2}.The pallets were then sintered at 860°C for 12 minutes within a gold capsule.Because Tl_2O_3 is a volatile material that melts at 717° C and evaporates with further heating, it was sintered in a gold capsule to keep it from escaping. Finally, $(Cu_{1/2}Tl_{1/2})Ba_2(Ca_{2-x}K_x)Cu_3O_{10-\delta}$(x=0, 0.5, 1, 1.5) superconducting samples were achieved. The doping concentration was controlled by the calculation of the precursor in the first step. In the doped samples, the amount of $Ca(NO_3)_2$ was reduced in the calculation and replaced by KOH.

4.2.1 X-ray diffraction scan

The crystal structure of the samples was measured by X-ray diffraction scan (XRD) by employing Bruker DX 8 Focus and CuKα radiations of wavelength 1.54056 °A. A computer refinement program (check cell) was used for determining the unit cell parameters.

4.2.2 Four probe resistivity

The temperature-dependent resistivity of the samples was measured using a ”four point/probe” apparatus. Four contacts are made at the flat surface of the sample, the contacts are made by the silver paste so it may not break when the sample is cooled to a very low temperature. The temperature is lowered down to 78 K using liquid nitrogen. A current around (1-2 mA) is passed through the outer probes and induces a voltage in the inner voltage probes. The temperature is raised slowly from 78K to room temperature, simultaneously measuring the current (I) and voltage (V) across the probes by the Keithley-2400 source meters. Finally resistivity is plotted across each Kelvin using the formula

$$\rho(T) = \frac{VA}{IL}$$

Here L and A is the length and the area of the sample.

4.2.3 Fourier Transform infrared spectroscopy

The absorption measurements were carried out by using Nicolet 5700 Fourier Transform Infrared Spectrometer (FTIR) in the wavenumber rnge of 400-700cm^{-1}.

4.2.4 Scanning electron microscopy (SEM)

The electron micrographs of our samples were taken in JEOL JSM-7610F Field Emission SEM, which offers magnification with 2000 X resolution at 15 kV, making it possible to observe the fine surface morphology of our samples.

4.3 Results and Discussion

Figure4.1 (a) shows the X-ray diffraction spectra of $(Cu_{1/2}Tl_{1/2})Ba_2(Ca_{2-x}K_x)Cu_3O_{10-\delta}$(x=0, 0.5, 1, 1.5) samples, the strong crystalline structure of these samples is confirmed by the prominent peaks in the spectra.These samples followed the orthorhombic crystal structure and Pmmm space group [15,22]. All the peaks were fitted by cell refinement computer software checkcell. Figure 4.1 (b,c) shows the parameters of the unit cell calculated after carefully analyzing the peaks of the X-ray diffraction spectra.

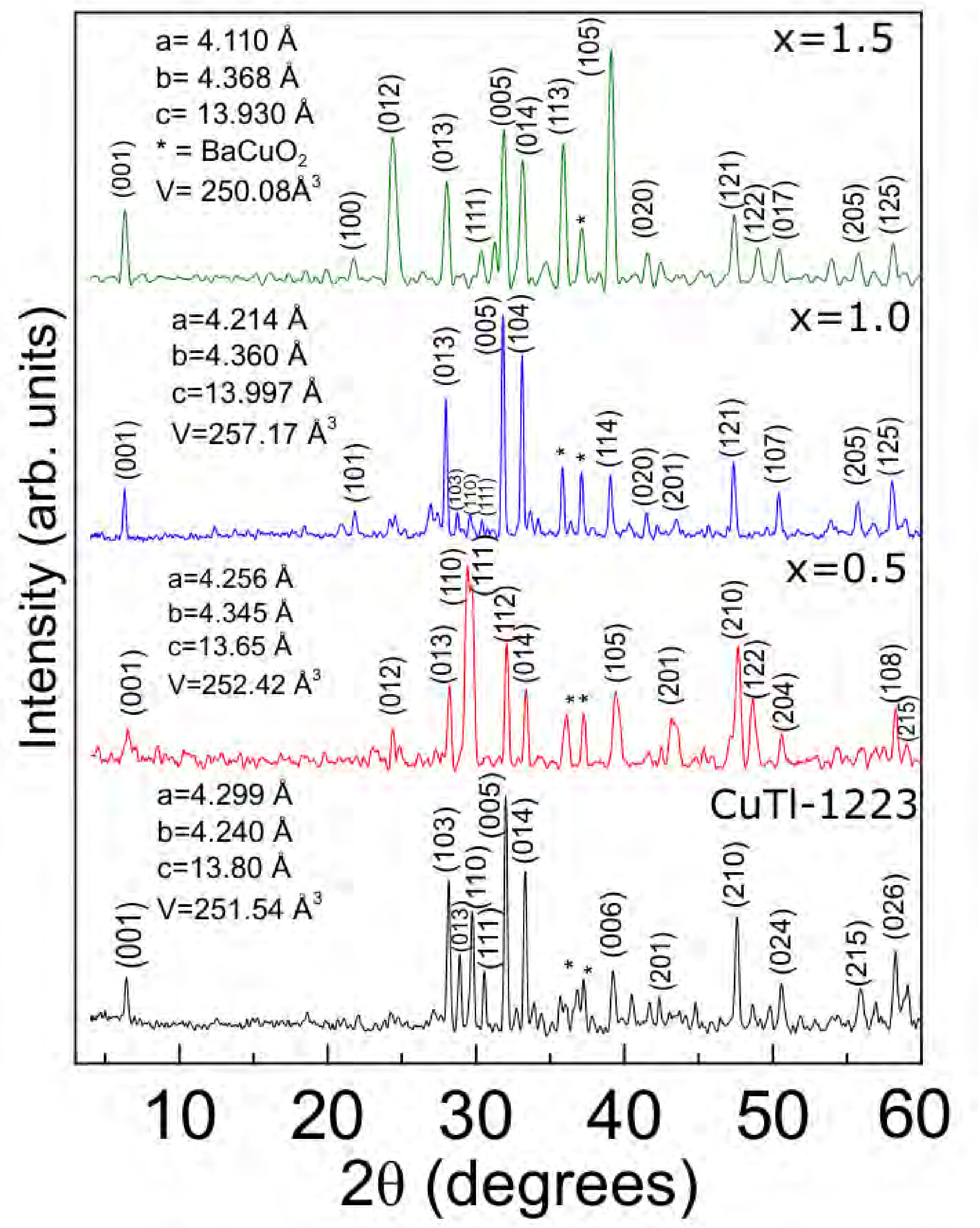

Fig 4.1:(a)X-Ray diffraction spectra of $(Cu_{1/2}Tl_{1/2})Ba_2(Ca_{2-x}K_x)Cu_3O_{10-\delta}$(x=0, 0.5, 1, 1.5) composites

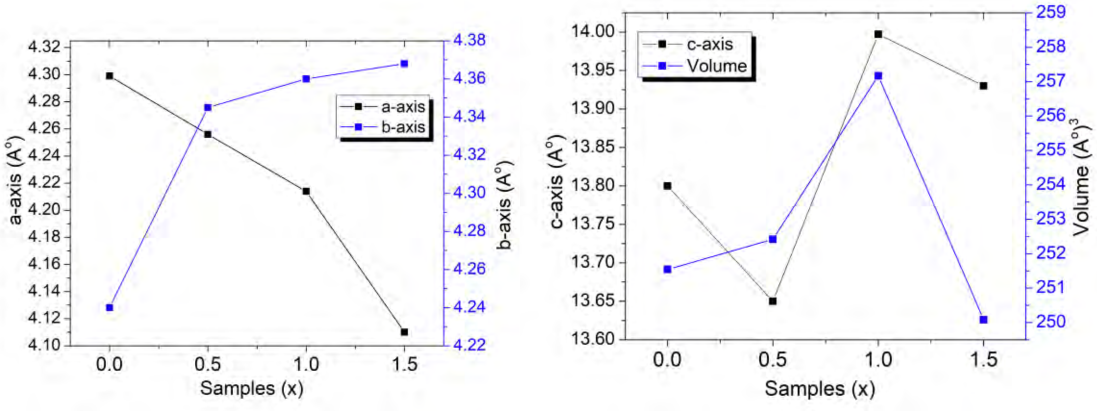

Fig 4.1:(b) Comparison of a and b axis.**(c)**The c axis and volume comparison.

Potassium doping causes an initial increase in the c-axis length and unit cell volume, which is followed by a subsequent decrease as K doping is increased to 50% in$(Cu_{1/2}Tl_{1/2})Ba_2(Ca_{2-x}K_x)Cu_3O_{10-\delta}$(x=0, 0.5, 1, 1.5)compounds. It is most likely that the less electronegative K (0.82) compared to Ca (1.0) promotes relaxation of crystal lattice axes and the volume of the unit cell [23]. The a-axis length subsequently increases and the b-axis length decreases with the doping of K in the final compound see Figure 4.1(c). Here it is important to note that the peaks observed around $2\theta = 36^\circ$ and 37° are due to the excess unreacted $BaCuO_2$ impurity which is common in the CuTl-1223 phase [24,25]. The melting point of $BaCuO_2$ is higher than 1000˚C so it is impossible to get rid of these impurity phases at our synthesis temperature.

The resistivity measurements of $Cu_{1/2}Tl_{1/2})Ba_2(Ca_{2-x}K_x)Cu_3O_{10-\delta}$(x=0, 0.5, 1, 1.5) samples from room temperature 90 (K) down to 78 K are presented in figure 2 (a). The magnification near the critical regime (transition regions) is depicted in Figure 2(b). These samples revealed zero resistivity i.e critical temperature (Tc) at 100K, 100 K, 88 K, and 94 K, respectively.

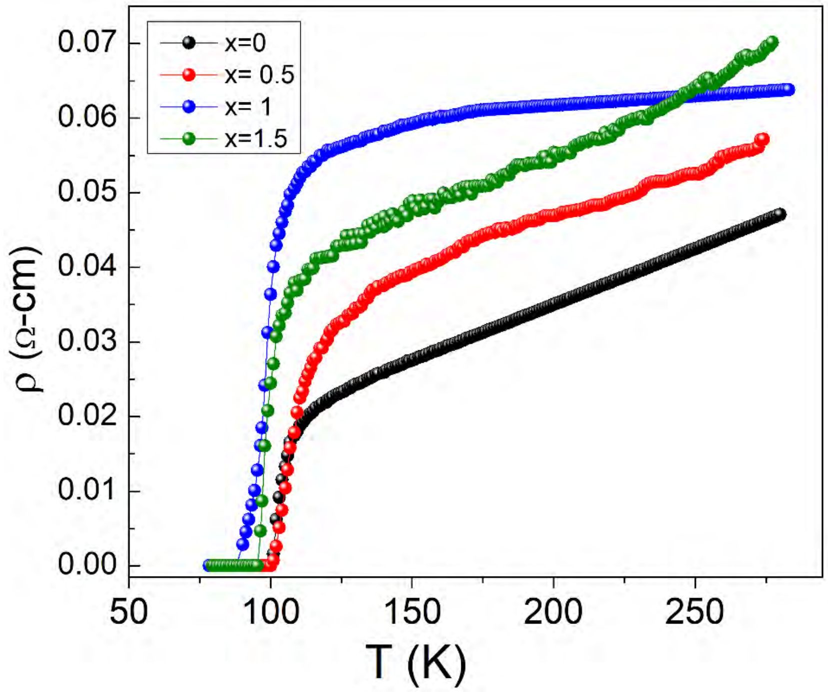

Fig 4.2:(a) Resistivity patterns of $(Cu_{1/2}Tl_{1/2})Ba_2(Ca_{2-x}K_x)Cu_3O_{10-\delta}$(x=0, 0.5, 1, 1.5) composites

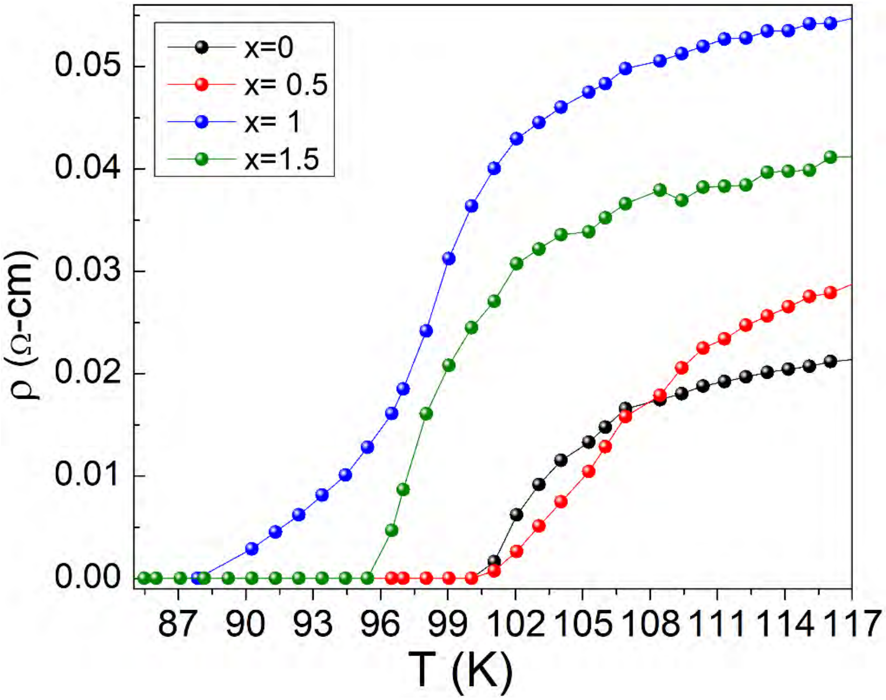

Fig4.2(b) Zoon in view Resistivity vs. temperature plots near critical regions.

With the doping of K in the final product, the value of the room temperature resistivity increases see Table 4.1. The metallic resistivity of these CuTl-based superconductor samples frequently fluctuates from room temperature through the onset of superconductivity.

Sample	**Resistivity**		
	T_C (R=0) K	**T_C (Onset) K**	**Resistivity room temperature(Ω- cm)**
X=0	100	112	0.047
X=0.5	100	119	0.059
X=1	88	109.4	0.15
X=1.5	94	108.4	0.071

***Table No 4.1**: Resistivity data of $Cu_{1/2}Tl_{1/2})Ba_2(Ca_{2-x}K_x)Cu_3O_{10-\delta}$(x=0, 0.5, 1, 1.5)*

The onset of superconductivity in $Cu_{1/2}Tl_{1/2})Ba_2(Ca_{2-x}K_x)Cu_3O_{10-\delta}$(x=0, 0.5, 1, 1.5) samples is observed around 112 K, 119 K, 109.4 and 108.4 K, respectively. The decrease in the T_c(R=0K) and the T_c (onset) with the doping of Potassium is due to the weaker interplanar coupling caused by doping of larger ionic size K atom (0.133 nm) compared to Ca (0.099 nm). Also, the difference in masses in Ca and K atoms at the interplane sites adds its part in reducing the superconducting properties of these materials [26].

The phonon modes related to the vibrations of oxygen atoms in the unit cell of $(Cu_{1/2}Tl_{1/2})Ba_2(Ca_{2-x}K_x)Cu_3O_{10-\delta}$(x=0, 0.5, 1, 1.5) samples were studied by the Fourier transform infrared spectroscopy (FTIR) absorption measurements (figure 4.3(a)). There are two noticeable absorption modes linked to the vibrations of apical oxygen atoms of type Tl-O_A-Cu(2) and Cu(1)-O_A-Cu(2) which were observed around 420 and 536cm^{-1}. One CuO_2 planer oxygen mode is also observed at 590-580 cm^{-1},see figure4.3(b) [27,28].

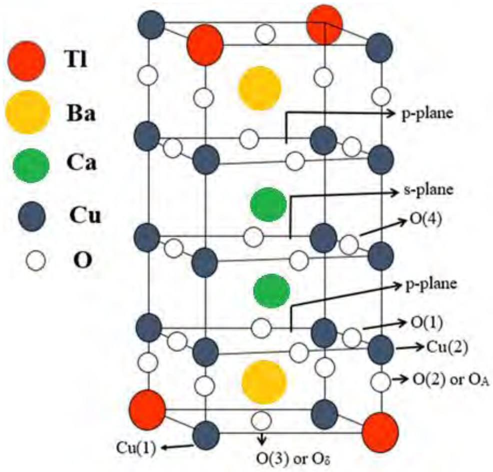

Fig 4.3 (a): Phonon modes related to the vibrations of $Cu_{1/2}Tl_{1/2}Ba_2Ca_2Cu_3O_{10-\delta}$ unit cell

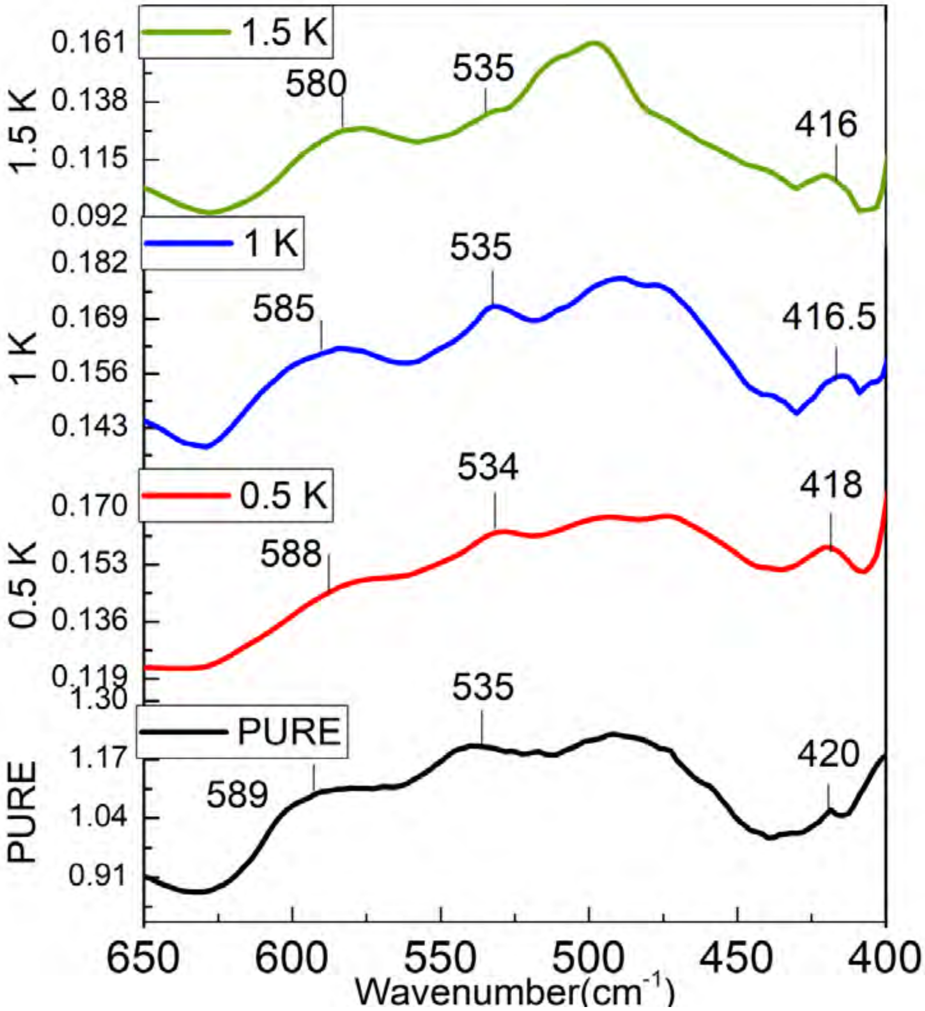

Fig 4.3(b): FTIR absorption spectra of $(Cu_{1/2}Tl_{1/2})Ba_2(Ca_{2-x}K_x)Cu_3O_{10-\delta}$(x=0, 0.5, 1, 1.5) samples

The apical oxygen mode of type Cu(1)-O_A-Cu(2) is softened from 420 cm^{-1} to 414 cm^{-1} with the doping of potassium in the final compound (figure 4.4 (b)). However, K doping has a small impact on the peak location of other oxygen modes. The rise in the c-axis is most likely caused by an increase in the charge reservoir layer, which increases the bond length of Cu(1)-O_A-Cu(2) and hence softens the apical oxygen mode. The CuO_2 planer oxygen mode is softened from 589 $cm^{-1}$to 580 cm^{-1} with the doping of K. This softening in the planar oxygen phonon mode is attributed to the smaller mass of K in comparison to Ca. The softening of this mode also indicates that the K has been substituted at the Ca interplane locations, increasing the interplane distance and hence decreasing the interplanar coupling. [26].

The scanning electron micrographs of these samples is shown in Figure 4.4. Here it can be seen that with the doping of potassium the grain size increases and the pinning centers starts filling which is most likely due to smaller size of K atoms compared to Ca atoms.

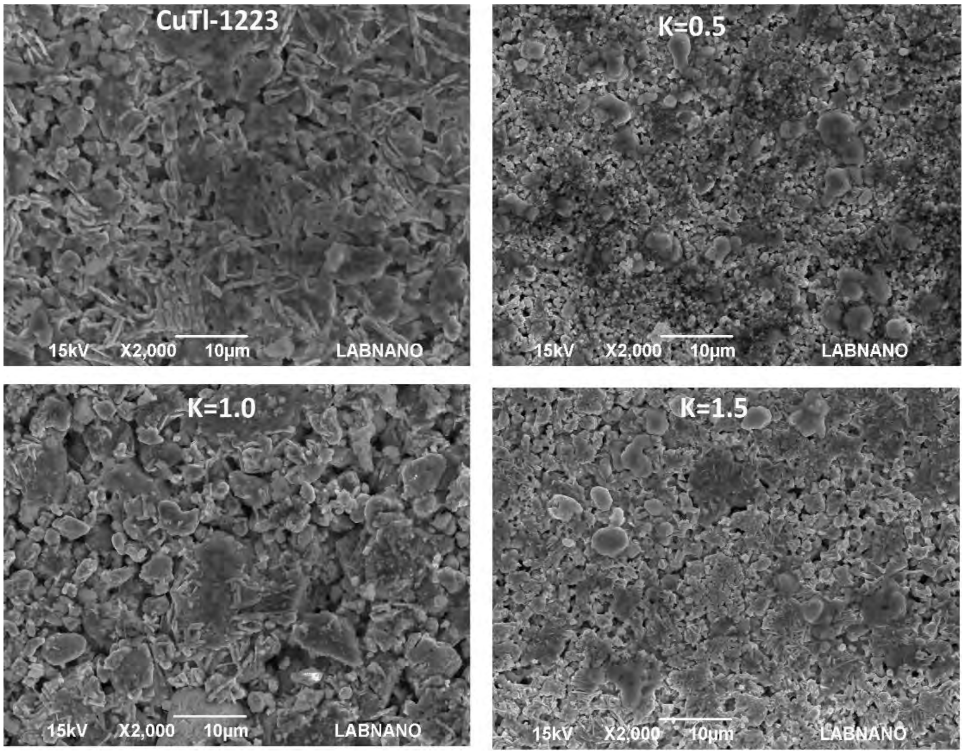

Fig 4.4: Scanning electron micrographs (SEM)of $(Cu_{1/2}Tl_{1/2})Ba_2(Ca_{2-x}K_x)Cu_3O_{10-\delta}$(x=0, 0.5, 1, 1.5) samples

Here we would like to mention that we have also prepared $(Cu_{1/2}Tl_{1/2})Ba_2(Ca_{2-x}K_x)Cu_3O_{10-\delta}$(x=2) sample i.e Calcium free sample but it doesn't form a stable structure. Some amorphous phases were observed in the XRD spectrum and the resistivity measurements also don't show any superconducting signs. From here we have concluded that the phase structure of CuTl-1223 is unstable without the presence of Calcium atom.

4.3.1 Excess conductivity analyses

To ascertain the crucial inherent superconducting properties in such materials, the excess conductivity investigations are necessary. Equations are used to perform the analysis for the research of Cooper-pair creation and their function in the mechanism of high temperature superconductivity in these materials:

$$\Delta\sigma(T) = \Delta\sigma_{RT}\varepsilon^{-\lambda_D} \qquad (1)$$

This equation can be modified in form of:

$$\ln \Delta\sigma(T) = \ln \Delta\sigma_{RT} - \lambda_D \ln(\varepsilon) \qquad (2)$$

Here $\varepsilon = \left[\frac{T - T_c^{mf}}{T_c^{mf}}\right]$ is the reduced temperature and λ_D is a dimensional exponent that determines the severity of numerous thermally activated methods, where λ_{cr}=0.3 refers to the slope below T_G corresponding to the critical regime, λ_{3D}=0.5 above $T_G$corresponding to the three-dimensional conductivity, the λ_{2D}=1.0 to the slope value above T_{3D-2D} that is associated with the two-dimensional conductivity and λ_{0D}=2 to the conductivity, not in any particular direction [29-32]. λ_D along with the values 0.3, 0.5, 1.0 and 2.0 is for the critical, three-dimensional (3D), two-dimensional (2D) and zero-dimensional (0D) conductivity respectively [33-38].We used the Lawrence and Doniach (LD) model to analyse the conductivity data acquired from our polycrystalline samples. T_{cmf} is the mean-field critical temperature below this temperature mean-field critical theory is applicable. T_{cmf} can be derived by taking the derivative of resistivity ($d\rho/dT$) the peak point of the $d\rho/dT$ graph represents T_{cmf}. The general formula connecting the excess conductivity versus reduced temperature follows as[39,40]:

$$\Delta\sigma_{LD} = [e^2/(16\hbar d)](1+J\varepsilon^{-1})^{-1/2}\varepsilon^{-1} \quad (3)$$

Here the "$\xi_{c(0)}$" is a coherence length along the c-axis, J= $\{2\xi_{c(0)}/d\}^2$ is the inter-layer coupling and "d" is the thickness of superconducting layers.

The $\ln\Delta\sigma_{(T)}$ versus $\ln(\varepsilon)$ graphs and the intersection of several dimensional exponents are used to determine the cross-over temperatures of various conductivity processes. The coherence length along the c-axis $\xi_{c(0)}$ have been evaluated using crossover temperatures of the two- and three-dimensional conductivity regimes, respectively, i.e. T_{3D-2D}:

$$T_{3D-2D} = T_c\,[1+(2\xi_{c(0)}/d)^2] \quad \ldots\ldots\ldots\ldots\ldots (4)$$

After determining $\xi_c(0)$ using the preceding expression, the inter-layer coupling J and Fermi velocity v_F of superconducting carriers are obtained using the following formulas:

$$v_F = \frac{5\pi k_B T_c \xi_{c(0)}}{2K\hbar} \ldots\ldots\ldots\ldots\ldots(5)$$

$$J = \{2\xi_{c(0)}/d\}^2 \ldots\ldots\ldots\ldots\ldots (6)$$

The proportionality co-efficient obtained for the preceding formulation of v_F is $K \cong 0.12$ [37].Despite suppression in the values of coherence along c-axis $\xi_{c(0)}$, the inter-layer coupling value J, the value of Fermi velocity v_F, the values for thermodynamic critical field B_c, These parameters are determined by using the temperature of onset of critical regime T_G, Ginzburg Landau number (N_G) and by using the Ginzburg-Landau theory making use of the underlying equations [32-35]:

$$N_G = \left|(T_G - T_C)/T_C\right| = 0.5[K_B T_c / B_{c(0)}^2 \gamma^2 \xi_{c(0)}^3]^2 \quad (7)$$

$$B_c = \frac{\Phi_0}{2\sqrt{2}\pi\lambda_{p.d(0)}\xi_{ab(0)}} \ldots\ldots\ldots\ldots(8)$$

$$B_{c1} = \frac{B_c}{\kappa\sqrt{2}}\ln\kappa \quad \ldots\ldots\ldots\ldots\ldots\ldots(9)$$

$$B_{c2} = \sqrt{2}\kappa B_c \quad \ldots\ldots\ldots\ldots\ldots\ldots (10)$$

$$J_c = \frac{4\kappa B_{c1}}{3\sqrt{3}\lambda_{p.d(0)}\ln\kappa} \ldots\ldots\ldots\ldots\ldots (11)$$

In these expressions $\kappa=\lambda/\xi$ is the Ginzburg Landau parameter 'GL'. The phase relaxation time of Cooper-pair $\tau_\varphi$is estimated by [36-38]

$$\tau_{\phi} = \frac{\pi\hbar}{8k_B T\varepsilon_0} \text{ .... (12)}$$

The energy required to break apart the Cooper-pairs is found by using the following equation:

$$E = \frac{h}{\tau_{\phi}(1.6\times10^{-19})} \text{(eV) .... (13)}$$

All the samples were chosen for the excess conductivity analyses.

4.3.2 Excess Conductivity Analyses of $(Cu_{1/2}Tl_{1/2})Ba_2(Ca_{2-x}K_x)Cu_3O_{10-\delta}$(x=0, 0.5, 1, 1.5) samples

The $\ln\Delta\sigma_{(T)}$ versus ln(ε) plot of $(Cu_{1/2}Tl_{1/2})Ba_2(Ca_{2-x}K_x)Cu_3O_{10-\delta}$(x=0, 0.5, 1, 1.5) samples are shown in Figure 4.5(a,b,c,d). Each figure's inset shows the derivative of resistivity in the transition regime. All the plots were carefully analyzed to find the slopes of different conductivity regimes. After carefully fitting the slopes we found the cross-over of critical and three-dimensional conductivity regimes T_G in these samples are around 102.5 K, 106.1 K, 99.9 K, and 97.3 K, the cross-over of three-dimensional conductivity regime and two-dimensional conductivity regime $T_{3D\text{-}2D}$ are around 104.4 K, 107.4 K, 103 K and 99.9 K and the cross-over temperature of two-dimensional conductivity regime and the zero-dimensional conductivity regime $T_{2D\text{-}0D}$ arises between 106.4 K, 113.4 K, 104.1 K and 101.3 K respectively. The mean-field critical temperatures in these samples are 102 K, 105 K, 99 K and 96 K respectively see table 4.2.

After calculating the superconducting parameters from the formulas discussed above it is determined that the coherence length along the c-axis $\xi_{c(0)}$, and the london penetration depth $\lambda_{p.d}$ increase after doping of potassium and keep increasing as we increase the doping concentration of potassium, see table 4.3. This shows that with the doping of the K at the Ca site the thickness of the interplaner layers increases thereby making the efficient transfer of the charge carriers to the conducting planes and hence increasing the density of the charge carrier in the conducting CuO_2 planes [41]. The phase relaxation time of the carriers decreases substantially whereas the energy required to break apart the Cooper pairs increases with the K doping in the final compound (table

4.3). A subsequent decrease in the population of pinning centers, most likely causes the decrease in carrier lifetime.

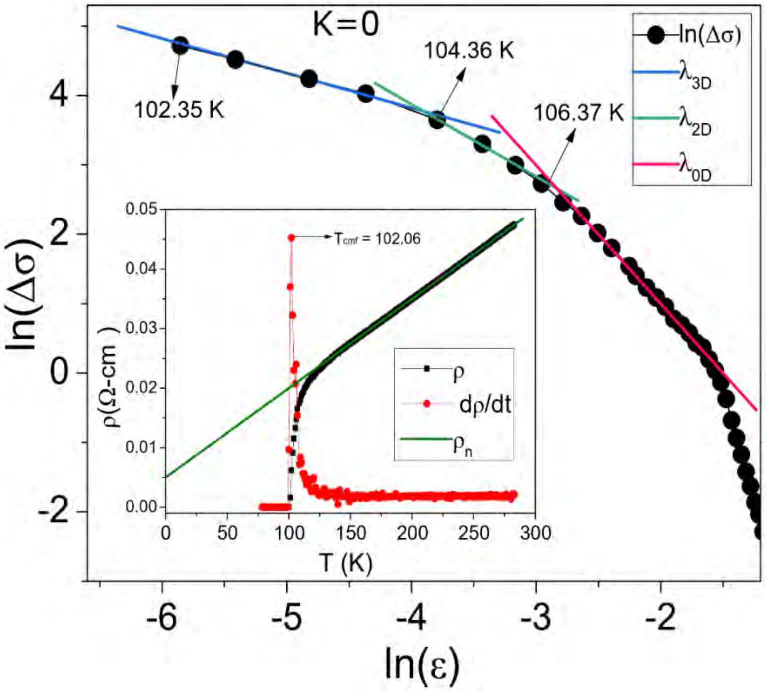

Fig 4.5 (a):ln(Δσ) versus ln(*ε*) depiction of $(Cu_{1/2}Tl_{1/2})Ba_2Ca_2Cu_3O_{10-\delta}$

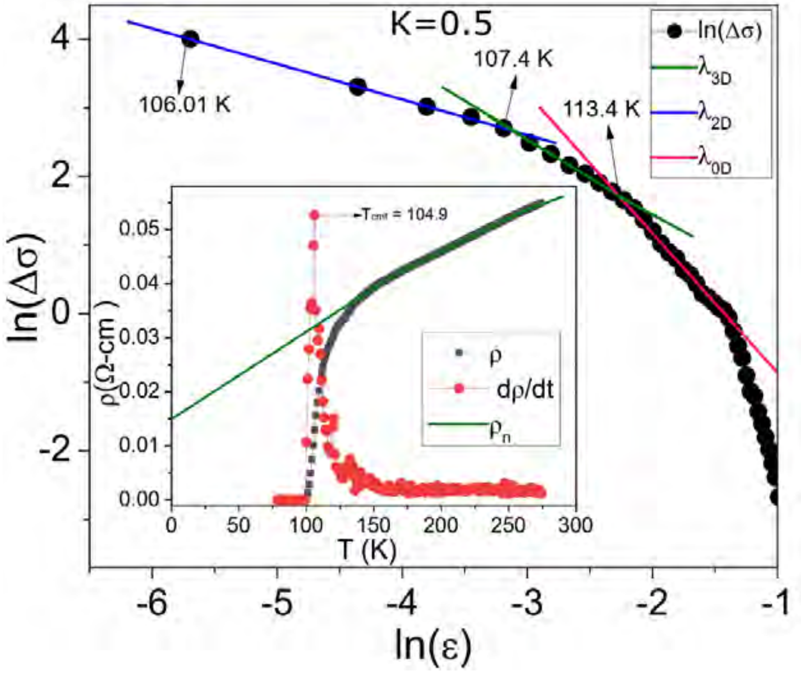

Fig 4.5 (b): ln(Δσ) versus ln(*ε*) depiction of $(Cu_{1/2}Tl_{1/2})Ba_2(Ca_{1.5}K_{0.5})Cu_3O_{10-\delta}$

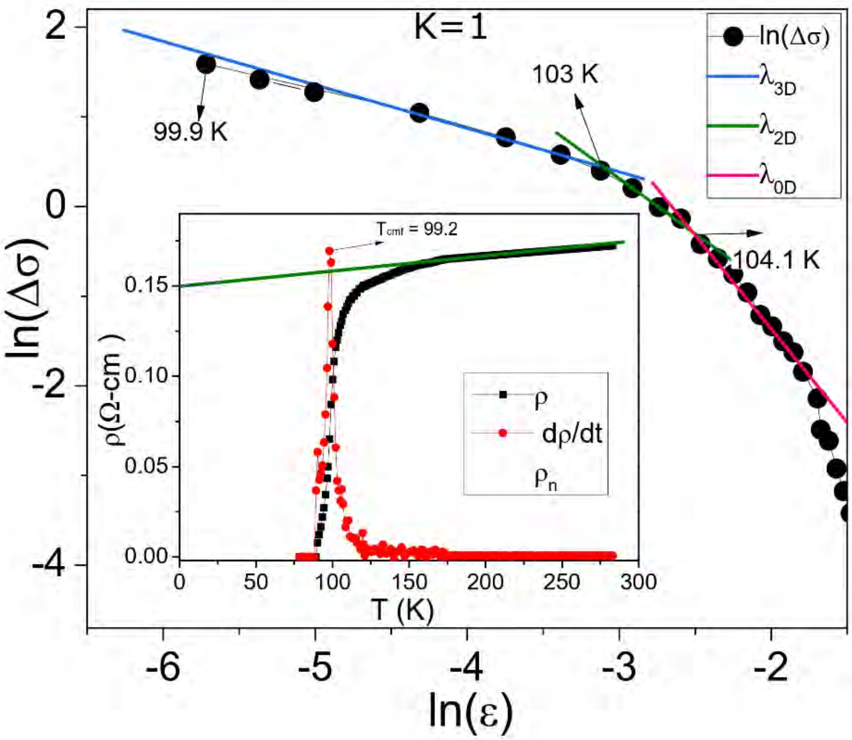

Fig 4.5 (c): ln(Δσ) versus ln(ε) depiction of $(Cu_{1/2}Tl_{1/2})Ba_2(Ca_1K_1)Cu_3O_{10-\delta}$

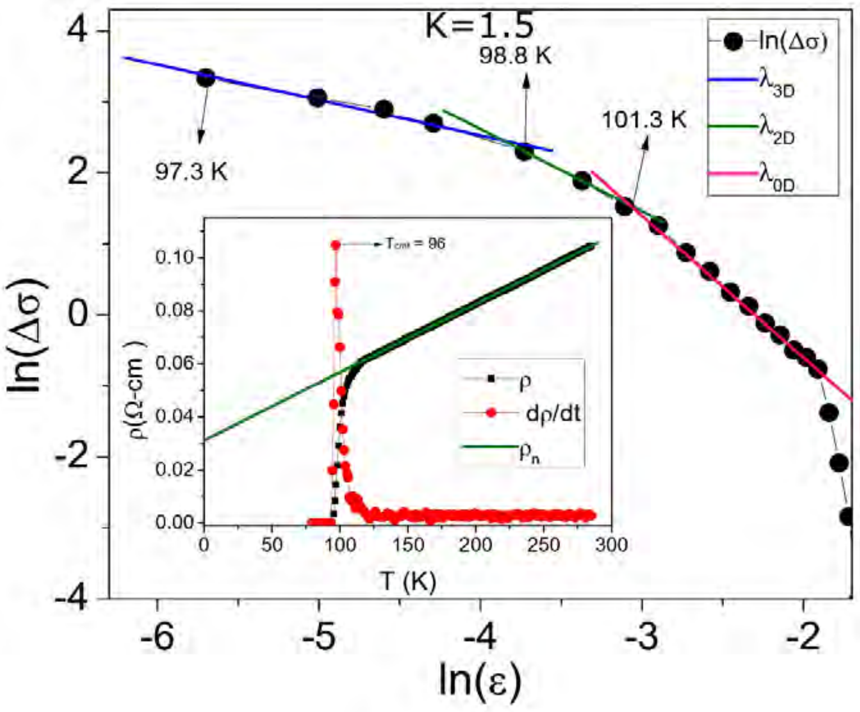

Fig 4.5(d): ln(Δσ) versus ln(ε) depiction of $(Cu_{1/2}Tl_{1/2})Ba_2(Ca_{0.5}K_{1.5})Cu_3O_{10-\delta}$

The values of parameters such as B_{c0}(T), B_{c1}(T), J_c(0) are decreased with the increased K doping in $(Cu_{1/2}Tl_{1/2})Ba_2(Ca_{2-x}K_x)Cu_3O_{10-\delta}$(x=0, 0.5, 1, 1.5) samples, demonstrating how doping changes the material's weak magnetic flux pinning regime. A good explanation for this hypothesis is the healing effect introduced by smaller-sized Potassium atoms compared to Calcium which most likely eliminates the microscopic pinning centers, this hypothesis is also supported by the SEM images as explained earlier in figure 4.4. A possible decreased population of microscopic pinning centers suppresses the values aforementioned parameters. With the doping of K in the final compound, this might also be interpreted as an increase in London penetration depth $\lambda_{p.d}$ and the Ginzburg Landau (GL) parameter κ [42].

Sample	**λ_{3D}**	**λ_{2D}**	**λ_{0D}**	**$T_{CR\text{-}3D}=T_G$ (K)**	**$T_{3D\text{-}2D}$ (K)**	**$T_{2D\text{-}0D}$ (K)**	**T_c^{mf}(K)**	**T^* (K)**	**$\alpha=\rho_n(0K)$ (Ω-cm)**
Pure	0.5	1	2	102.5	104.3	106.4	102.1	131	1.34
0.5 K	0.52	0.98	2.15	106	107.4	113.4	104.9	149	.47
1 K	0.56	1.05	2	99.9	103	104.1	99.2	142	1.06
1.5 K	0.51	0.99	1.99	97.3	99.8	101.3	96	114	1.52

Table 4.2:*Parameters estimated from diagram of ln(Δσ) versus ln(ε)*

Sample	**$\xi_c(0)$ (Å)**	**J**	**N_G**	**$\lambda_{p.d}$ (Å)**	**$B_{c(0)}$ (T)**	**B_{c1} (T)**	**B_{c2} (T)**	**κ**	**$J_{c(0)}$ x10^3 (A/cm^2)**	**V_F x 10^7 (m/s)**	**E_{Break} (eV)**	**τ_φ x 10^{-13} (s)**
Pure	1.13	0.022	0.004	184.1	7.909	1.187	128.7	11.506	23.360	9.65	0.009	4.49
0.5 K	1.15	0.023	0.011	237.3	6.135	0.788	128	14.833	14.056	9.86	0.039	1.04
1 K	1.47	0.038	0.007	324.5	4.487	0.470	128.9	20.280	7.520	11.22	0.023	1.73
1.5 K	1.52	0.041	0.014	399.5	3.644	0.332	128.2	24.971	4.960	12.3	0.010	4.1

Table 4.3: *Parameters estimated from excess conductivity analysis of* $(Cu_{1/2}Tl_{1/2})Ba_2(Ca_{2-x}K_x)Cu_3O_{10-\delta}$*(x=0, 0.5, 1,1.5)*

Conclusions

In summary, we have replaced Potassium with Calcium atoms in the interplanar sites of CuTl-1223 superconductors by synthesizing $(Cu_{1/2}Tl_{1/2})Ba_2(Ca_{2-x}K_x)Cu_3O_{10-\delta}$(x=0, 0.5, 1, 1.5). The as-prepared samples were then characterized by:X-ray diffraction, 4-probe resistivity, scanning electron microscopy, and FTIR absorption. Furthermore, excess conductivity analysis was used to study the impact of K doping on the mechanism of superconductivity. The X-ray diffraction spectra shows that these samples followed the orthorhombic crystal structure and Pmmm space group. We found out that Potassium doping causes an initial increase in the c-axis length and unit cell volume, which is followed by a subsequent decrease as K doping is increased to 50% inthe final compounds. This behavior is due to the less electronegativity of K compared to Ca atoms. A subsequent decrease in the T_c(R=0K) and the T_c (onset) with the doping of potassium observed which is due to the weaker interplanar coupling caused by doping of larger ionic size K atom compared to Ca. The apical oxygen mode of type Cu(1)-O_A-Cu(2) is softened from 420 cm^{-1} to 414 cm^{-1} with the doping of K in the final compound with the doping of K, as observed in the FTIR absorption measurements. It is most likely that the increase in the c-axis takes place in the charge reservoir layer blocks which elongates the bond length of Cu(1)-O_A-Cu(2) and hence the softening of this apical oxygen mode. The softening of CuO_2 planer oxygen mode also shows that the K has been substituted at the Ca interplane sites thereby increasing the interplane distance and hence the weakening of the interplaner coupling. The superconducting parameters were calculated by carrying out the excess conductivity analysis by using AL and LD model. The coherence length along the c-axis $\xi_{c(0)}$, and the London penetration depth $\lambda_{p.d}$ increase after doping of potassium and keep increasing as we increase the doping concentration of potassium. From here we can say the doping of the K at the Ca site the thickness of the interplaner layers increases thereby making the efficient transfer of the charge carriers to the conducting planes and hence increasing the density of the charge carrier in the conducting CuO_2 planes. The values of parameters such as B_{c0}(T), B_{c1}(T), J_c(0) are decreased with the increased K doping in $(Cu_{1/2}Tl_{1/2})Ba_2(Ca_{2-x}K_x)Cu_3O_{10-\delta}$(x=0, 0.5, 1, 1.5) samples. This is because a smaller sized K causes the healing effect which reduces the microscopic pinning centers which was also confirmed by the scanning electron micrographs. A possible decreased population of microscopic pinning centers suppresses the values of these parameters. Finally, we have concluded that the interplanar coupling plays a vital role in the mechanism of high-temperature superconductivity which could be disturbed even by a slight change in mass and the electronegativity of a doped atom.

References

[1] K. ALEX MÜLLER AND J. GEORG BEDNORZ, The Discovery of a Class of High-Temperature Superconductors, *SCIENCE.* 4 Sep 1987 Vol 237, Issue 4819 pp. 1133-1139.

[2] Zhou, X., Lee, WS., Imada, M. *et al.* High-temperature superconductivity. *Nat Rev Phys* 3, 462–465 (2021).

[3] José A. Flores-Livas, Lilia Boeri, Antonio Sanna, Gianni Profeta, Ryotaro Arita, Mikhail Eremets, A perspective on conventional high-temperature superconductors at high pressure: Methods and materials, Physics Reports, Volume 856, Pages 1-78, ISSN 0370-1573, (2020) https://doi.org/10.1016/j.physrep.2020.02.003.

[4] Zhang J, Wu H, Zhao G, Han L, Zhang J. A Review on Strain Study of Cuprate Superconductors. Nanomaterials (Basel). 2022 Sep 25;12(19):3340.

[5] R. N. Bhattacharya, R. D. BlaugherThallium-Based High-Tempature Superconductors. 1st Edition, Published1993 ImprintCRC Press, ISBN 9781003067160.

[6]Kanwal, A., Khan, N.A., Garcia, F. *et al.* Carrier Transport Enhancement by Doping Rubidium in $Cu_{0.5}Tl_{0.5}$-1223 Superconducting Phase. *JOM* (2023).

[7] M. Rahim and N.A. Khan, Study of Mg-doped (Cu0.5Tl0.5) Ba2(Ca2 − yMgy)(Cu2.5Cd0.5)O10 − δ (y= 0, 0.05, 0.1, 0.25, 0.5, 0.75,1.0) superconductors. *J. Alloys Compd.* 572, 74 (2013).

[8] S. Ismail, A.K. Yahya, and N.A. Khan, Influence of Ce substitution at Sr-site on superconducting fluctuation behavior and infrared absorption of Tl0.9Bi0.1Sr2− x Cex Ca0.9Y0.1Cu1.99Fe0.01O7− δ

(x= 0–0.20) ceramics. *J. Supercond. Novel Magn.* 25, 1849 (2012).

[9] C. Park, R.L. Synder, Structures of High-Temperature Cuprate Superconductors, J. m. Ceram. Soc. 78, 3171 (1995)

[10]N.A.KhanandA.A.Khurram,EnhancedsuperconductingpropertiesofCu$_{1-x}Tl_xBa_2Ca_{2-y}Mg_yCu_3O_{10-\delta}$(y=0,0.5,1.0,and1.5),Appl.Phys.Lett.,86(15):1–3, (2005).

[11]N. A. Khan and G. Husnain, Superconductivity in Be substituted by Ca in $Cu_{0.5}Tl_{0.5}Ba_2Ca_{n-1-y}Be_yCu_nO_{2n+4-}$(n = 3, 4andy = 0.7, 1.5, 1.7, 2.0). Physica C Supercond. Its Appl., 436(1) : 51 (2006).

[12]B. Shabbir, X. Wang, S. R. Ghorbani, C. Shekhar, S. Dou & O. N. Srivastava, Hydrostatic pressure: A very effective approach to significantly enhance critical current density in granular iron pnictide superconductors. *Scientific Reports* volume 5, Article number: 8213 (2015).

[13]B. Shabbir, H. Huang, C. Yao, Y.Ma, S. Dou, T.H. Johansen, H. Hosono, and X. Wang, Evidence for superior current carrying capability of iron pnictide tapes under hydrostatic pressure. Phys. Rev. Materials 1, 044805.

[14]A. Raza, N. A. Khan, N. Hassan, Enhanced Anharmonic Oscillations in $Cu_{0.5}Tl_{0.5}Ba_2(Ca_{2-y}Mg_y)Cu_{3-x}Cd_xO_{10-\delta}$ (y = 0, 1; x = 0, 1.5) Superconductors, Journal of Electronic Materials. 49, 2302 (2020).

[15]K. Naseem, N. A. Khan, S. H. Safeer, Effect of Magnesium Doping to Reduce the Charge Reservoir Layer in $Cu_{0.5}Tl_{0.5}(Ba_{2-x}Mg_x)Ca_2Cu_3O_y$ (x = 0, 0.15, 0.25, 0.35) Superconductors. Journal of Electronic Materials. 50, 2164 (2021).

[16]B. Shabbir , M. I. Malik, N. A. Khan, Effect on Diamagnetism and Phonon Modes due to Mg and Be Doping at Ca Sites in $Cu_{0.5}Tl_{0.5}Ba_2Ca_{3-y}M_yCu_4O_{12-\delta}$ (y = 0 and 1.5 for M = Mg, Be) High-Temperature Superconductors, J Supercond Nov Magn. 24, 1977 (2011).

[17]Safeer, S.H., Riaz, A. & Khan, N.A. Study of Carrier Transfer Mechanism When Substituting Strontium at Barium Sites in CuTl-1223 Superconducting Phase. *J. Electron. Mater.* 50, 4034–4040 (2021).

[18] Arif, M., Rahim, M., Hassan, N. et al. Enhanced superconducting properties of Ti doped (Cu0.5Tl0.5)Ba2(Ca2−xTix)Cu3O10−δ samples. J Mater Sci: Mater Electron 29, 12414–12418 (2018). https://doi.org/10.1007/s10854-018-9357-9

[19] N. A. Khan and A. A. Khurram, Study of the intergranular coupling of $Cu_{0.5}Tl_{0.5}Ba_2Ca_{2-y}Mg_yCu_3O_{10-\delta}$ (y = 0, 0.5, 1.0 and 1.5) superconductors. Appl. Phys. Lett. 86, 152502 (2005).

[20] Nawazish Khan, M. U. Muzaffar, Decoupling of the CuO 2 plane and superconductivity in Cu0.5Tl0.5Ba 2 (Ca2−ySry)Cu 3 O10−δ(y = 0–0.4) samples, May 2016 International Journal of Modern Physics 30(17):1650097

[21] N. A. Khan and G. Husnain, Superconductivity in Be substituted by Ca in Cu0. 5Tl0. 5Ba2Can− 1− yBeyCunO2n+ 4− δ (n= 3, 4 and y= 0.7, 1.5, 1.7, 2.0), Physica C 436, 51 (2006).

[22] A. Kanwal, N.A. Khan, Excess Carrier Density and the Role of Spin Density Waves in the Mechanism of High Tc Superconductivity in (Cu0.5Tl0.5)Ba2Ca2Cu3-xKxO10-δ (x = 0, 1, 2, 2.5, 3) Samples. J. Electron. Mater. 52, 602–612 (2023). https://doi.org/10.1007/s11664-022-10032-y.

[23] Dong X, Oganov AR, Cui H, Zhou XF, Wang HT. Electronegativity and chemical hardness of elements under pressure. Proc Natl Acad Sci U S A. 2022 Mar 8;119(10):e2117416119. doi: 10.1073/pnas.2117416119. Epub 2022 Mar 1. PMID: 35238642; PMCID: PMC8915985.

[24]A.Raza,S.H.Safeer,a nd N.A.Khan,The Role of Mass of Doped Atoms in the Superconductivity of $Cu_{0.5}Tl_{0.5}Ba_2Ca_2Cu_3O_{10d}$and $Cu_{0.5}Tl_{0.5}Ba_2Ca_2Cu_{1.5}$ $M_{1.5}O_{10d}$ (M = Cd, Zn, and Ni). J.Supercond. Nov. Magn., 30(5), 1153 (2017).

[25] Lai, C.C., Ho, P.C., Hung, C.Y., Ku, H.C., Chinese Journal of Physics **29**(1) (1991).

[26] Arif, M., Rahim, M., Hassan, N. *et al.* Enhanced superconducting properties of Ti doped $(Cu_{0.5}Tl_{0.5})Ba_2(Ca_{2-x}Ti_x)Cu_3O_{10-\delta}$ samples. *J Mater Sci: Mater Electron* **29**, 12414–12418 (2018). https://doi.org/10.1007/s10854-018-9357-9.

[27] N. A. Khan, M. Mumtaz, K. Sabeeh, M. I.A. Khan, and M. Ahmed, The studyofphononmodesof$Cu_{1-x}Tl_xBa_2Ca_3Cu_4O_{12-y}$superconductorthinfilmsbyFTIR absorption spectroscopy.Phys. C Supercond. its Appl., 407(3-4):103 (2004).

[28] M. U. Muzaffar, S. H. Safeer, N. A. Khan, A.A. Khurram, Modified synthesis route to achieve Sr substituted $Cu_{0.5}Tl_{0.5}$-1234 superconductor phase, Materials Chemistry and Physics,Volume 181,384-390, (2016).

[29] B. Shabbir, A. Ullah, N. Hassan. M. Irfan, N. A. Khan. Suppression of Superconductivity Due to Enhanced Co Doping in $Cu_{0.5}Tl_{0.5}Ba_2Ca_2Ca_2Cu_{3-y}Co_yO_{10-\delta}$ Superconductors. *J Supercond Nov Magn.* 24, 1521–1526 (2011).

[30] E. Kandyel, M.A. Sekkina, M.A.T. Dawoud, M.Y Bohnam, Effect of 3d metal ion doping on the structure and superconductivity of $(Tl_{0.5}Pb_{0.5})Sr_2CaCu_2O_7$. *Solid State Commun.*135, 214-219 (2005).

[31] N. A. Khan, N. Hassan, S. Nawaz, B. Shabbir, S. Khan, A. A. Rizvi, Effect of Sn substitution on the para-conductivity of polycrystalline $Cu_{0.5}Tl_{0.5}Ba_2Ca_2Cu_{3-y}$ $Sn_yO_{10-\delta}$superconductors. *Journal of Applied Physics.*107, 083910 (2010).

[32]M. Kaur, R. Srinibasan, G. K. Mehta, D. Kanjilal, R. Pinto, S.B. Ogale, S. Mohan,V. Ganesan, Effect of disorder on the exponent in the coherence region in high temperature superconductors. *Physica C*, 443 61-68 (2006).

[33] M. ME. Barakat, A. I. Abou-Aly, R.Awad, N. S. Aly and S. Ibrahim, Excess conductivity analysis for $Y_{3-x}Nd_xBa_{5-x}Ca_xCu_8O_{18-\delta}$superconducting phase.*International Journal of Modern Physics B.* Vol. 30, 1650115 (2016).

[34]N. A. Khan, S. H.Safeer, M. Rahim, M.Nasir Khan, andN. Hassan. Excess Conductivity Analysis of $Cu_{0.5}Tl_{0.5}Ba_2Ca_{n-1}Cu_nO_{2n+4-\delta}$ $(n = 2, 3, 4)$ Thin Films. *J Supercond Nov Magn* **30,** 1493–1498 (2017).

[35]N. A. Khan,S.H.Safeer,M. N. Khan,M. Rahim,andN. Hassan. Excess conductivity analyses of $(Cu_{0.5}Tl_{0.5})Ba_2Ca_3Cu_4O_{12-\delta}$ thin film samples synthesized at different temperatures and post-annealed in flowing nitrogen atmosphere. *J Mater Sci: Mater Electron.* 29, 2209–2215 (2018).

[36] S. H. Safeer, A. Riaz, N.A. Khan. Study of Carrier Transfer Mechanism When Substituting Strontium at Barium Sites in CuTl-1223 Superconducting Phase. *Journal of ElecMateri.* 50, 4034–4040 (2021).

[37]K.Naseem, N. A. Khan, S. H.Safeer, Effect of Magnesium Doping to Reduce the Charge Reservoir Layer in $Cu_{0.5}Tl_{0.5}(Ba_{2-x}Mg_x)Ca_2Cu_3O_y$ (x = 0, 0.15, 0.25, 0.35) Superconductors. *Journal of ElecMateri*. 50, 2164–2170 (2021).

[38] W.E. Lawrence and S. Doniach, Proceedings of the Twelfth International Conference on Low Temperature Physics, edited by Eizo Kanda (Keigaku, Tokyo) p. 361, (1971).

[39] N. Hassan, B.Shabbir, N. A. Khan, Excess-conductivity analysis of Mg- and Be-doped polycrystalline $Cu_{0.5}Tl_{0.5}Ba_2Ca_{1.5}M_{1.5}Cu_4O_{12-}$(M=0, Be, Mg) superconductors, *Journal of Applied Physics*. 105, 083926 (2009).

[40]Abu Aly, A.I., Ibrahim, I.H., Awad, R.A., El-Harizy, A.: Stabilization of Tl-1223 Phase by Arsenic Substitution. *J. Supercond. Nov. Magn.*23, 1325–1332 (2010).

[41] Hebard, A., Rosseinsky, M., Haddon, R. *et al.* Superconductivity at 18 K in potassium-doped C_{60}. *Nature* **350**, 600–601 (1991).

[42] Shengnan Zhang, C. Li, Qingbin Hao, Xiaobo Ma, Tianni Lu and Pingxiang Zhang, Optimization of Bi-2212 high temperature superconductors by potassium substitution, 2015 *Supercond. Sci. Technol.* 28 045014.